Development of a virtual optimized chemistry method. Application to hydrocarbon/air combustion

Melody Cailler, Nasser Darabiha, Benoit Fiorina

Development of a virtual optimized chemistry method. Application to hydrocarbon/air combustion

Mélody Cailler [a,b,*], Nasser Darabiha [a], Benoît Fiorina [a]

[a] Laboratoire EM2C, CNRS, CentraleSupélec, Université Paris-Saclay, 3, Joliot Curie, Gif-sur-Yvette 91192, France
[b] SAFRAN Tech, Modelling & Simulation, Rue des Jeunes Bois, Châteaufort, 78114 Magny-les-Hameaux, France

ABSTRACT

Chemical flame structures encountered in practical turbulent combustion chambers are complex because multiple regimes such as premixed, stratified or diffusion may coexist. Combustion modeling strategies based on single flame archetype fail to predict pollutant species, such as CO. To account for multiple combustion regimes, at a reduced computational cost, a novel approach based on virtual optimized mechanisms is developed. This method consists in (i) building a kinetic scheme from scratch instead of reducing a detailed mechanism, (ii) using a reduced number of virtual reactions and virtual species that do not represent real entities and (iii) using sub-mechanisms dedicated to the prediction of given flame quantities. In the present work, kinetic rate parameters of the virtual reactions and virtual species thermodynamic properties are optimized through a genetic algorithm to properly capture the flame temperature as well as CO formation in hydrocarbon/air flames. The virtual optimized chemistry approach is first applied to the derivation of methane/air reduced kinetic schemes. The flame solutions obtained with the virtual optimized mechanisms are subsequently compared to the reference flame library showing good predictive capabilities for both premixed and non-premixed flame archetypes. Analysis of the impact of the reference database demonstrated that the quality of CO formation modeling depends on the reference flame library used to train the optimized kinetic scheme. The virtual mechanisms are also tested on 2-D partially-premixed burners showing good agreement between the reference mechanism and the reduced virtual schemes. Finally, the virtual optimized chemistry approach is used to derive virtual optimized mechanisms for heavy fuels oxidation.

1. Introduction

The conflicting nature of performance, operability and environmental constraints leads engine manufacturers to perform a fine optimization of the burner geometry to find the best design compromise [1]. Numerical simulation constitutes an attractive tool to achieve this challenging task, and is routinely used in design offices to capture macroscopic flow features. However, the modeling of combustion chemistry in complex reactive flow environment is still a critical issue to properly predict the pollutant formation in practical configurations. A precise and comprehensive description of the reacting chemical system may be achieved by using detailed kinetic schemes, involving hundreds of species and thousands of reactions. Unfortunately, the application of such models in simulations of real scale configurations is prohibitive. The computational cost associated with the resolution of species transport equations, the numerical stability issues due to reaction rates stiffness and the potential modeling issues related to the coupling with turbulence, limit the use of detailed schemes to simple geometries and light fuels. To take into account kinetic effects in simulations of real combustion chambers two modeling challenges must be addressed [2]. First, a combustion chemistry model imposing low computational costs and allowing a precise description of chemical effects of interest must be provided. Then, an adequate turbulent combustion model is required to account for the interactions between the sub-filter scale turbulent eddies and the resolved flame front. This work will focus on this first point.

Among existing kinetic reduction technique, a widely used approach to model complex chemistry at a low computational cost is tabulated chemistry. This strategy assumes that the flame structure can be parametrized by a reduced set of control parameters [3–6]. The chemical response of a canonical problem is stored in a database as a function of representative variables. This method is very efficient to capture the chemical structure when

the combustion regime is well identified. However, when stratified or partially-premixed flames are encountered tabulated chemistry methods based on single flame archetype fail to predict the inner flame structure and minor species such as CO [7,8]. Also, the simultaneous treatment of heat losses, multiple fuel inlets or dilution by hot gases can lead to difficulties to identify the control parameters and the flame prototypes combining these effects.

Alternatives to tabulated chemistry are "chemistry-driven" reduction approaches based on skeletal reduction [9–11] and Quasi-Steady State (QSS) approximation [12–14]. The resulting kinetic schemes, called analytically-reduced mechanisms, provide an accurate description of the flame structure and intermediate species on a wide range of conditions [15,16]. Recently, the simulation of the swirled SGT-100 burner [17] demonstrated the capabilities of analytic chemistry to capture CO and NO_x concentrations in a representative configuration. Nevertheless, the computational cost associated with this methodology can be high, in particular if heavy hydrocarbon molecules such as soot precursors (PAH) are targeted or if the oxydation of hybrid multi-component fuels is addressed. A new chemistry modeling approach combining (i) identification of chemical trajectories accessed in the target configuration, (ii) application of chemical reduction methods and (iii) optimization of kinetic rate parameters has recently been proposed [18]. Even though this approach allows higher reduction rates than classical chemistry reduction techniques, the question of the cost associated with the prediction of heavy molecules is still unanswered.

A third approach to account for kinetic effects relies on semi-global mechanisms composed by few major species interacting through a reduced number of global reactions. These kinetic schemes are calibrated to reproduce global flame quantities of interest such as: adiabatic flame temperature, laminar premixed flame speed or auto-ignition delay times [19–21]. During the last 40 years, numerous semi-global kinetic schemes were developed. First works by Westbrook and Dryer [19] or Jones and Lindstedt [20] exploited the two layers flame structure of hydrocarbon/air flames to derive two- and four-step generic mechanisms. More recently, Franzelli et al., [21] developed an empirical method to build two-step mechanisms valid on a wide range of operating conditions. In this work, pre-exponential factors are tabulated as a function of the local equivalence ratio to fit laminar flame speed, and reaction orders of reactants are selected so as to account for the impact of pressure on the laminar flame speed. With the increase of computational power, fully automated methods based on evolutionary optimization algorithms have arisen to determine optimum chemical rate parameters of semi-global schemes [22–25]. Independently of the calibration approach used, semi-global schemes are cost-effective and efficiently capture global flame properties. As such they are widely used for simulations of large scale combustion systems [26–28]. Unfortunately, these low-order mechanisms are not able to capture the inner flame structure and complex chemistry phenomena such as flame ignition or extinction. Moreover, as few intermediate species are included, pollutant formation processes are not accounted for.

An alternative method, based on virtual optimized schemes, has been proposed to address combustion chemistry over both premixed and non-premixed flame regimes, at a reduced computational cost [29]. This strategy, aiming at building reaction mechanisms capable of describing user-defined flame properties, relies on the optimization of a virtual mechanism composed of virtual reactions and virtual species whose thermodynamic properties are also calibrated. Virtual optimized mechanisms capabilities to capture temperature and heat release rate on premixed and non-premixed combustion regimes have been validated on 1-D laminar flames [29]. Interestingly, an original optimization method has also been lately introduced to derive one-step schemes using one virtual product with optimized properties [30]. The resulting one-step mechanisms retrieve well global flame properties of both premixed (burnt gas temperature, laminar consumption speed and thermal thickness) and diffusion (extinction strain rate) flames.

The present paper focuses on the development of a low-CPU cost virtual chemistry approach dedicated to the prediction of minor species formation in premixed and non-premixed hydrocarbon/air flames. A special emphasis is given to CO concentration prediction which is of particular interest for industrial applications and from a modeling point view, as CO formation features both fast and slow processes. Moreover influence of the reference database used to optimize the virtual scheme is discussed. In a first part, the general methodology for the derivation of both the main and satellite virtual optimized mechanisms is presented. The new chemistry description method is first used to derive virtual reduced schemes dedicated to the prediction of the flame temperature and CO concentration in methane/air flames. The subsequent virtual mechanisms are compared against main chemistry description approaches in terms of predictive capabilities, computational costs and numerical stiffness. In a fourth part, fully resolved simulations of a two-dimensional laminar partially-premixed methane/air burner are performed to assess virtual optimized schemes capabilities in a multi-dimensional context. Finally, virtual optimized kinetic schemes devoted to the description of heavy fuels oxidation are built-up and compared to detailed chemistry solutions.

2. Methodology for building up virtual kinetic schemes

2.1. Virtual chemistry concept

The virtual reaction mechanism is optimized to predict specific flame properties requested by a Research and Development engineer on an ensemble of user-defined flame configurations. The properties of interest may be for instance the flame temperature, the consumption speed and the formation of a given pollutant (CO, NO_x, soot precursors, etc.). The target flame prototypes must be representative of the variety of combustion elements encountered in practical applications. In the present work, the optimized scheme targets both premixed and non-premixed adiabatic flame archetypes so that complex flame structures are captured. The reference database could however be enlarged by adding other reactive configurations such as 0-D homogenous reactors or non-adiabatic flames, if these combustion events occur in the targeted application.

The virtual mechanisms are generated through an original method relying on:

- Building up a reduced chemical mechanism from scratch instead of reducing a detailed scheme. Most reduction techniques are based on progressive elimination of species and reactions so as to achieve a satisfactory level of accuracy compared to the complex chemistry. Conversely, virtual optimized chemistry approach gradually increases the number of species and reactions so that the target flame quantities are properly described.
- Using virtual global reactions that do not model real kinetic paths between species. Virtual optimized mechanism may be seen as a mathematical architecture designed to retrieve a set of user-defined physical targets.
- Using virtual species whose physical properties (thermodynamic and transport) are optimized to capture real mixture averaged properties. In opposition with classical reduction methods [19,20] that use real species, species do not represent real chemical entities but are considered as degrees of freedom of the model. It must however be underlined that when minor species such as pollutants are targeted the virtual mechanism involves virtual species that model the real chemical compound of interest.
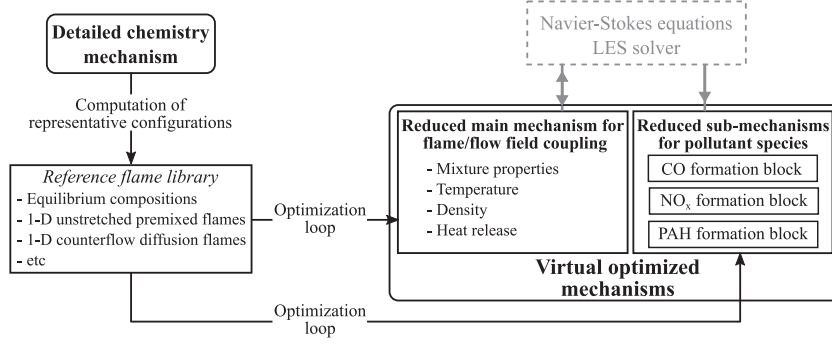
Fig. 1. Virtual optimized mechanisms architecture.

The virtual optimized mechanisms architecture is illustrated in Fig. 1. The proposed strategy consists in building and optimizing independent reduced virtual kinetic schemes dedicated to the capture of a given flame property. The virtual optimized mechanisms are decomposed into a main kinetic scheme and several satellite sub-mechanisms dedicated to minor species description.

Both main and sub-schemes are trained through genetic optimization to recover a target database composed of reference solutions representative of different canonical combustion problems. The main virtual mechanism is calibrated to capture the flame/flow field coupling. More precisely, the main kinetic scheme aims at describing the mixture-averaged thermodynamic and transport properties as well as the heat released by combustion. As the main virtual scheme is trained to capture the flame structure of a complex chemistry database, it accounts for the overall impact of all species present in the reference scheme on the heat release rate, within a certain accuracy. However, as only integrated quantities such as temperature and mixture-averaged properties are targeted, individual species informations are not modeled by the main virtual scheme. To have access to species concentration of interest (*e.g.* CO, CO_2, NO_x or HC_x) satellite-mechanisms are introduced. These sub-schemes, exclusively designed to model individual species concentrations, do not retro-act on the main virtual scheme. No feedback from satellite mechanisms to the main virtual scheme is indeed required as detailed chemistry information are included in the heat release and temperature profiles predicted by the main virtual scheme.

Reduced virtual schemes (including main mechanism and sub-mechanisms) have a structure similar to conventional mechanisms. In this article, the superscript v refer to quantities associated to virtual species and reactions whereas the superscript d denotes detailed chemistry formalism. A detailed mechanism involving N_s^d species of chemical symbols $\mathcal{V}_k^d$ interacting through N_r^d reactions is formulated as follows:

$$\sum_{k=1}^{N_s^d} \alpha_{k,r}^{'d} \mathcal{V}_k^d \rightarrow \sum_{k=1}^{N_s^d} \alpha_{k,r}^{''d} \mathcal{V}_k^d \qquad \text{for } r = 1, \ldots, N_r^d \tag{1}$$

where $\alpha_{k,r}^d$ are the stoichiometric coefficients per mass unit. Similarly, the virtual mechanism reads:

$$\sum_{k=1}^{N_s^{v_q}} \alpha_{k,r}^{'v_q} \mathcal{V}_k^{v_q} \rightarrow \sum_{k=1}^{N_s^{v_q}} \alpha_{k,r}^{''v_q} \mathcal{V}_k^{v_q} \qquad \text{for } r = 1, \ldots, N_r^{v_q} \tag{2}$$

where the superscript v_q identifies the qth virtual mechanism with $q = m$ for the main virtual mechanism and $q = s_n$ for the nth virtual sub-mechanism for CO, PAH or NO_x for instance.

Using the notation $d_t f = \partial_t f + \partial_{x_i}(f u_i)$, the systems of conservation equations associated to both main and satellite mechanisms may be written as:

Main mechanism:

$$d_t \rho = 0$$

$$d_t(\rho u_j) = \partial_{x_i} \sigma_{ij}$$

$$d_t(\rho Y_k^{v_m}) = -\partial_{x_i}(\rho Y_k^{v_m} V_{k,i}^{v_m}) + \dot{\omega}_k^{v_m} \qquad \text{for } k \in [1, N_s^{v_m}]$$

$$d_t(\rho h) = \partial_{x_i}\left(\lambda^v \partial_{x_i} T - \rho \sum_{k=1}^{N_s^{v_m}} Y_k^{v_m} V_{k,i}^{v_m} h_k^{v_m}\right) \tag{3}$$

nth satellite-mechanism:

$$d_t(\rho Y_k^{v_{s_n}}) = -\partial_{x_i}(\rho Y_k^{v_{s_n}} V_{k,i}^{v_{s_n}}) + \dot{\omega}_k^{v_{s_n}} \qquad \text{for } k \in [1, N_s^{v_{s_n}}] \tag{4}$$

where ρ is the density, u_i the velocity component and σ_{ij} the sum of the viscous tensor τ and the hydrodynamic pressure P tensor. Y_k is the kth species mass fraction, while $V_{k,i}$ and $\dot{\omega}_k$ denote the molecular diffusion velocity component and the chemical reaction rates of the kth species. In the enthalpy conservation equation, λ is the thermal conductivity and T denotes the temperature.

The main virtual model, trained to describe the flame/flow field interactions, is coupled with the flow governing equations through mass, species, momentum and energy conservation equations. Unlike the main mechanism, the satellite sub-mechanisms are not involved in the closure of mass, momentum and energy equations but only account for pollutant species mass fractions. The temperature, density and mixture properties (heat capacity, enthalpy, conductivity, *etc.*) evaluated from the main virtual mechanism are used as input in satellite kinetic models.

The procedure used for virtual mechanisms optimization is discussed in Section 2.2. The derivation of the main block is detailed in the Section 2.3, while the design of a sub-mechanism for CO prediction is discussed in Section 2.4.

2.2. Optimization procedure

One major ingredient of the strategy is the optimization of species physical properties and reaction rate parameters so as to accurately recover a set of target flame properties. This inverse problem expresses as a constraint minimization:

$$\begin{cases} \text{minimize} & \mathcal{E}\left(\mathbf{w}^v(\mathcal{X}^v), \mathbf{w}^d(\mathcal{X}^d)\right) \\ \text{submitted to} & \mathcal{S}(\mathbf{w}^v(\mathcal{X}^v)) \end{cases} \tag{5}$$

where $\mathcal{E}$ is the function comparing virtual and detailed solutions, often called fitness or cost function. The vector $\mathbf{w} = (\rho u, \rho v, \rho w, \rho Y_k, \rho h)$ refers to the state vector depending on the set of parameters $\mathcal{X}$ describing the thermo-chemochemical, transport and kinetic rate properties. Detailed state vector $\mathbf{w}^d$ and virtual state vector $\mathbf{w}^v$ are constrained by the set of conservation equations for mass, momentum and energy referred as $\mathcal{S}$:

$$\frac{\partial \mathbf{w}}{\partial t} + \nabla.\mathbf{F}(\mathbf{w}, \mathcal{X}) = \mathbf{s}(\mathbf{w}, \mathcal{X}) \tag{6}$$

where **F** is the flux tensor and **s** the source term vector.

Following the work of Polifke et al., [22], the identification of the best set of free parameters $\mathcal{X}^\nu$ is performed through an efficient and automated procedure. The following section briefly presents the main classes of optimization methods that may be used to close the virtual kinetic schemes.

2.2.1. Brief review of optimization techniques

Two main classes of optimization approaches may be identified in the literature: deterministic and stochastic methods. Deterministic optimization methods include all optimization algorithms using a specific rule to guide the evolution from one set of candidate parameters to another [31]. As an example, gradient-based approaches use the cost function and its gradient to identify a new set of optimum parameters. Optimization methods based on sensitivity analysis examine the Jacobian of the studied system to guide the search direction [32]. On the contrary, stochastic optimization strategies introduce randomness during the search process to improve the algorithm efficiency. The introduction of randomness may indeed avoids the convergence towards a local optimum and eventually allows to approach the best solution [33]. The family of stochastic search optimization methods includes a wide variety of algorithms going from simulated annealing to particle swarm or genetic optimization.

Depending on the problem treated, the two techniques can feature very different behaviors. In this work, as the cost function is evaluated through the resolution of a non-linear system of differential equations, it can feature multiple ridges and valleys as well as discontinuities (because of calculations non-convergence). With such complex and highly structured landscapes fitness functions, the use of stochastic optimization algorithms is required [34]. Among the various types of random search techniques, evolutionary algorithms have been largely used for the optimization of kinetic schemes [22,24,35,36]. One of the main advantages of this optimization algorithm is its ability to balance between space exploration (random search) and space exploitation (fitness function information) so as to converge towards the best global solution [37]. This efficient and robust optimization approach is considered here for the optimization of virtual mechanisms. The next section introduces the main principles of evolutionary algorithms.

2.2.2. Evolutionary algorithms

Evolutionary algorithms explore the domain by modeling biological evolution principles and hereditary laws. Following the evolutionary theory introduced by Darwin [38], a number of optimization algorithms based on this concept were introduced. In this work, optimization of species thermodynamic properties and reaction rate parameters is performed using the genetic algorithm proposed by Holland [39] and later modified by Goldberg [40]. The evolutionary algorithm principle implemented in the in-house optimization code is described in Fig. 2.

The main steps of the evolutionary algorithm may be summarized as follows:

1. In a first stage, the initial generation composed of a set of individuals, representing potential solutions, is randomly generated. Each individual is represented by a real vector also called chromosome whose values called gene correspond to the unknown parameters. Definition of the chromosomes for the calibration of the species thermodynamic properties and the kinetic parameters are given in Section 2.5.
2. Each individual (potential solution) of the first generation is then evaluated through the fitness function $\mathcal{E}$ that discriminates good solution candidates from the others.
3. The next step relies on population evolution through the application of three genetic operators:

(i) A selection procedure is used to identify the fittest individuals to be the survivor parents for the next generation. The selection operator is based on a k-tournament algorithm.
(ii) A crossover operation is then applied on a couple of randomly chosen parents. This genetic operator imitates the hereditary process that mixes parental qualities towards potential improvement of the offspring.
(iii) Eventually, mutation operation is randomly applied on children solutions to improve the population diversity.

4. The predictive capabilities of every individual of the children population is then evaluated by comparing reference solutions to those obtained with the corresponding virtual models.
5. Finally, a reduction or filtering operation relying on k-tournament selection is applied to the total population formed by the merging between the parents' population and the children' population. To ensure a constant improvement of the generations an elitist model is used.
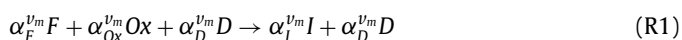
Details about initialization, selection procedure, genetic operators and elitism model are given in Appendix A. Evaluation of the virtual kinetic models is performed with the REGATH thermochemistry package [41].

2.3. Main virtual scheme for flame structure prediction

The general methodology to build up the main mechanism devoted to the description of flame/flow field coupling is presented. The structure of the virtual scheme is first introduced. Then, the optimization of virtual species properties and reaction rate parameters is discussed in Sections 2.3.2 and 2.3.4, respectively.

2.3.1. Main virtual mechanism generation principles

Two types of virtual mechanism structures composed of one or two consecutive virtual reactions have been tested in [29]. The two-step scheme is retained here because it provides a better description of the flame temperature profiles. This mechanism is composed of the two following consecutive virtual reactions:

$$\alpha_F^{\nu_m} F + \alpha_{Ox}^{\nu_m} Ox + \alpha_D^{\nu_m} D \rightarrow \alpha_I^{\nu_m} I + \alpha_D^{\nu_m} D \tag{R1}$$

$$I \rightarrow \sum_{k=1}^{N_p^{\nu_m}} \alpha_{P_k}^{\nu_m} P_k \tag{R2}$$

The first virtual reaction R1 converts fuel (F) and oxidizer (Ox) to an intermediate species (I) which is then transformed through reaction R2 into a set of N_p^ν virtual products P_k. The species named D is a dilutant compound which is not affected by chemical reactions.

Figure 3 illustrates the two consecutive steps required to build up the main virtual scheme. First, the thermo-chemical and transport properties of the virtual species are optimized to mimic real mixture properties such as heat capacity, heat conductivity and mixture-averaged molecular weight. Table (a) in Fig. 3 summarizes the physical properties optimized during the first stage of the procedure. The second step of the optimization aims at evaluating the kinetic rate constants of the virtual reactions (Table (b) in Fig. 3). The unknown parameters are fitted so that virtual scheme solutions are as close as possible to a set of reference flamelets obtained with a detailed chemistry mechanism. In the present study, the reference database is made of 1-D adiabatic laminar flames, either freely-propagating premixed or non-premixed counterflow.

The calibration of the main virtual scheme is performed step-by-step to minimize the total number of unknown that is identified at each step. The performance of the overall optimization procedure is therefore improved.
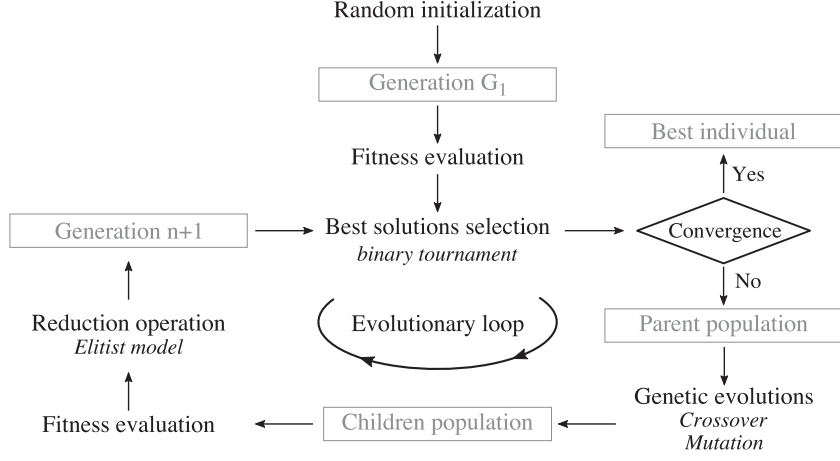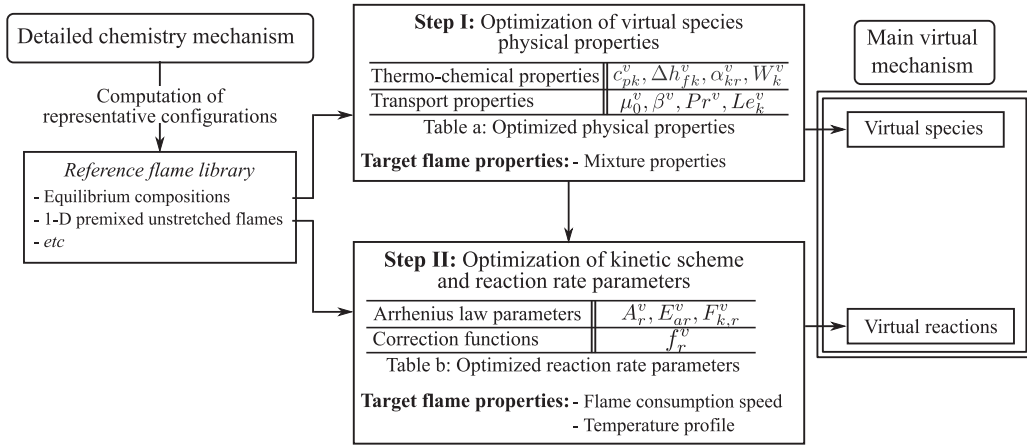
Fig. 2. Genetic algorithm principle.

Fig. 3. Main virtual optimized mechanism generation procedure.

2.3.2. Optimization of virtual species properties

In a first step, the thermodynamic and transport properties of the virtual species are calibrated to recover averaged properties of the multi-component real mixture.

Thermodynamic properties of reactant and product species: For both detailed and virtual formalisms, the quantity ψ is introduced to represent the mixture-averaged thermodynamic properties:

$$\psi^d = \sum_{k=1}^{N_s^d} \psi_k^d Y_k^d \quad \text{and} \quad \psi^{v_m} = \sum_{k=1}^{N_s^{v_m}} \psi_k^{v_m} Y_k^{v_m} \tag{7}$$

where the vector $\psi_k = \{h_k, c_{pk}\}$ gathers the enthalpy h_k and the heat capacity at constant pressure of the kth species. Following the NASA parametrization, c_{pk} and h_k are modeled by temperature dependent polynomial functions:

$$\frac{c_{pk}}{R} = a_{1k} + a_{2k}T + a_{3k}T^2 + a_{4k}T^3 + a_{5k}T^4 \tag{8}$$

$$\frac{h_k}{RT} = a_{1k} + \frac{a_{2k}}{2}T + \frac{a_{3k}}{3}T^2 + \frac{a_{4k}}{4}T^3 + \frac{a_{5k}}{5}T^4 + \frac{a_{6k}}{T} \tag{9}$$

The coefficients a_{lk} of species k correspond to thermodynamic coefficients. Classically, these coefficients are given in thermodynamic database built to retrieve the evolution of species individual properties with the temperature. In this work, the $N_T = 6$ coefficients a_{lk} of species k are optimized so that the real mixture properties are correctly described in both fresh and fully burnt gases where heat and mass diffusion may occur:

$$\psi^{v_m}|^f = \psi^d|^f \quad \text{and} \quad \psi^{v_m}|^{eq} = \psi^d|^{eq} \tag{10}$$

where superscripts f and eq denote fresh and equilibrium condition.

At this stage, evolution of the mixture thermodynamic properties (heat capacity and enthalpy) across the flame front is not explicitly targeted during the optimization process as the only local property considered is temperature. However, capability of the virtual scheme to capture mixture-averaged thermodynamic properties variation along the flame is *a-posteriori* verified.

The description of mixture-averaged properties in the fresh gases is achieved by attributing real properties to reactants (F and Ox) and dilutant (D) species of the virtual mixture:

$$\psi_A^{v_m} = \psi_A^d \quad \text{for } A = \{F, Ox, D\} \tag{11}$$

In practice, this condition is fulfilled by imposing real thermodynamic coefficients to virtual species:

$$a_{lA}^{v_m} = a_{lA}^d \quad \text{for } A = \{F, Ox, D\} \quad \text{and} \quad l \in [1; N_T] \tag{12}$$

For instance, for methane/air combustion, F, Ox and D have the thermo-chemical properties of CH_4, O_2 and N_2, respectively. In the following, the subset of species composed by fuel, oxidizer and dilutant species is referred as A.

The modeling of burnt gases thermodynamic properties is more complex as for hydrocarbon/air mixtures the equilibrium composition may involve hundreds of real species. To overcome this difficulty, the in-house genetic code presented in Section 2.2.2 is used to identify the minimum number of virtual products $N_p^{v_m}$ and their associated thermodynamic properties $a_{lP_k}^{v_m}$ that describe the most reliably the burnt gases state. This is achieved through the mini-

mization of the fitness function $\mathcal{E}_{\text{thermo}}^{\text{main}}$ defined as:

$$\mathcal{E}_{\text{thermo}}^{\text{main}}(\mathcal{X}) = \sum_{i=1}^{N_c}\left[\psi^{v_m}|^{eq}(\phi_i) - \psi^d|^{eq}(\phi_i)\right] \tag{13}$$

where $\mathcal{X}$ corresponds to the set of parameters to be optimized. N_c is the number of targeted operating conditions for instance the number of equivalence ratio conditions targeted in the flammability range $[\phi_L; \phi_R]$. Referring to reactions R1 and R2 and to Eq. (7), mixture-averaged thermodynamic properties ψ^d and ψ^{v_m} can be expressed by:

$$\psi^d = \sum_{k=1}^{N_s^d}\psi_k^d Y_k^d \tag{14}$$

$$\psi^{v_m} = \sum_{k\in A}\psi_k^{v_m}Y_k^{v_m} + \psi_I^{v_m}Y_I^{v_m} + \sum_{k=1}^{N_p^{v_m}}\psi_{P_k}^{v_m}Y_{P_k}^{v_m} \tag{15}$$

Accordingly to the structure of the two-step virtual mechanism, given by reactions R1 and R2, intermediate species fractions is null at equilibrium. By combining Eqs. (13)–(15), the fitness function describing the modeling of thermodynamic properties at equilibrium is given by:

$$\mathcal{E}_{\text{thermo}}^{\text{main}}(\mathcal{X}) = \sum_{i=1}^{N_c}\left[\sum_{k\in A}\psi_k^{v_m}Y_k^{v_m}|^{eq}(\phi_i) + \sum_{k=1}^{N_p^{v_m}}\psi_{P_k}^{v_m}Y_{P_k}^{v_m}|^{eq}(\phi_i)\right.$$
$$\left. - \sum_{k=1}^{N_s^d}\psi_k^d Y_k^d|^{eq}(\phi_i)\right] \tag{16}$$

Under equilibrium conditions, species mass fractions of virtual products are related to mass stoichiometric coefficients $\alpha_{P_k}^{v_m}$:

$$Y_{P_k}^{v_m}|^{eq} = \alpha_{P_k}^{v_m}Y_P^{v_m}|^{eq} \tag{17}$$

where $Y_P^{v_m}|^{eq} = \sum_{k=1}^{N_p^{v_m}}Y_{P_k}^{v_m}|^{eq}$ is the total mass fraction of virtual products in fully burnt gases. At equilibrium state, mass balance equation gives:

$$Y_P^{v_m}\Big|^{eq} = 1 - \sum_{k\in A}Y_k^{v_m}\Big|^{eq} \tag{18}$$

In real mixture, the equilibrium concentrations of product species depend on the initial temperature, pressure and composition of the fresh gases. To reduce the number of degrees of freedom, only equivalence ratio dependency is considered in the following. However, the formulation can be extended to pressure and fresh gases temperature dependency in a straightforward manner. To mimic equilibrium composition variations with equivalence ratio, the stoichiometric coefficients $\alpha_{P_k}^{v_m}$ are expressed as a function of the fresh gases composition. As a consequence, the set of parameters $\mathcal{X}$ to be optimized is defined as:

$$\mathcal{X} = \left\{N_p^{v_m}, \alpha_{P_k}^{v_m}(\phi_i), a_{lP_k}^{v_m}\right\} \quad \text{for} \quad \begin{cases} k\in\left[1; N_p^{v_m}\right] \\ i\in\left[1; N_c\right] \\ l\in\left[1; N_T\right] \end{cases} \tag{19}$$

Considering thermodynamic properties given by Eqs. (8) and (9) and identifying polynomial coefficients, one may express the fitness function of Eq. (16) as:

$$\mathcal{E}_{\text{thermo}}^{\text{main}}\left(N_p^{v_m}, \alpha_{P_k}^{v_m}(\phi_i), a_{lP_k}^{v_m}\right)$$
$$= \sum_{i=1}^{N_c}\sum_{l=1}^{N_T}\left[\bar{a}_{lA}^{v_m}|^{eq}(\phi_i) + \bar{a}_{lP}^{v_m}|^{eq}(\phi_i) - \bar{a}_l^d|^{eq}(\phi_i)\right] \tag{20}$$

The mixture-averaged coefficients $\bar{a}_l$ refer to the linear combination of the thermodynamic coefficients a_{lk} for each group of species:

$$\bar{a}_{lA}^{v_m}|^{eq}(\phi_i) = \sum_{k\in A}a_{lk}^{v_m}Y_k^{v_m}|^{eq}(\phi_i) \tag{21}$$

$$\bar{a}_{lP}^{v_m}|^{eq}(\phi_i) = \sum_{k=1}^{N_p^{v_m}}a_{lP_k}^{v_m}\alpha_{P_k}^{v_m}Y_P^{v_m}|^{eq}(\phi_i) \tag{22}$$

$$\bar{a}_l^d|^{eq}(\phi_i) = \sum_{k=1}^{N_s^d}a_{lk}^d Y_k^d|^{eq}(\phi_i) \tag{23}$$

The practical resolution of the optimization problem is detailed in Appendix B.

Thermodynamic properties of intermediate species: As previously stated, the thermodynamic properties of the intermediate species have no impact on the equilibrium gas state. However, as the intermediate species I may feature high concentrations in the flame front the value of the NASA coefficients $a_{lI}^{v_m}$, modeling the species sensible and chemical energy, can influence the description of the inner flame structure. As a consequence, thermodynamic properties of the intermediate species must be carefully modeled. To reach a proper description of the temperature profiles, the coefficients $a_{lI}^{v_m}$ may be included in the set of coefficients to be optimized, similarly as reaction rate parameters (see Section 2.3.4).

Interestingly, the typical endothermic behavior observed in rich premixed flame fronts may be considered to reduce the number of parameters to be optimized. Detailed chemistry simulations show that in rich premixed hydrocarbon/air flames (for $\phi > \phi_{\mathcal{L}}$) the maximum flame temperature reached in the flame front is higher than the equilibrium temperature T_{eq} obtained in fully burnt gases. To properly capture this phenomenon, the standard enthalpy of formation of species I is chosen so that reaction R2 is exothermic for $\phi < \phi_{\mathcal{L}}$ and endothermic for $\phi > \phi_{\mathcal{L}}$. Figure 4 shows the evolution of the standard enthalpy of formation of the virtual products in burnt gases ($\Delta H_{f,P}^{v_m}|^{eq} = \sum_k^{N_p^{v_m}}Y_k^{v_m}|^{eq}\Delta H_{f,k}^{v_m}$) with the equivalence ratio for two mixtures at different operating conditions. For $\phi < \phi_{\mathcal{L}}$, the condition $\Delta H_{f,I}^{v_m} > \Delta H_{f,P}^{v_m}$ ensures an exothermic behavior of the reaction R2, while for $\phi > \phi_{\mathcal{L}}$ the relation $\Delta H_{f,I}^{v_m} < \Delta H_{f,P}^{v_m}$ implies that reaction R2 is endothermic. This condition allows to express the NASA coefficient $a_{6,I}$ as a function of the targeted standard enthalpy of formation and the coefficients modeling the sensible part of the energy:

$$a_{6I}^{v_m} = \frac{\Delta H_{f,I}^{v_m}}{R} - \left(a_{1I}^{v_m}T_0 + \frac{a_{2I}^{v_m}}{2}T_0^2 + \frac{a_{3I}^{v_m}}{3}T_0^3 + \frac{a_{4I}^{v_m}}{4}T_0^4 + \frac{a_{5I}^{v_m}}{5}T_0^5\right) \tag{24}$$

2.3.3. Specific gas constants

As the main virtual mechanism aims at describing the density profiles across a flame, the specific gas constant $r_k^{v_m}$ (or equivalently the molecular weight $W_k^{v_m}$) of the virtual species k must be identified so as to reproduce the reference mixture-averaged specific gas constant r^{v_m} (or equivalently the molecular weight W^{v_m}) in both fresh and burnt gases:

$$r^{v_m}|^f = r^d|^f \Rightarrow \sum_{k=1}^{N_s^{v_m}}r_k^{v_m}Y_k^{v_m}|^f = \sum_{k=1}^{N_s^d}r_k^d Y_k^d|^f \tag{25}$$

$$r^{v_m}|^{eq} = r^d|^{eq} \Rightarrow \sum_{k=1}^{N_s^{v_m}}r_k^{v_m}Y_k^{v_m}|^{eq} = \sum_{k=1}^{N_s^d}r_k^d Y_k^d|^{eq} \tag{26}$$
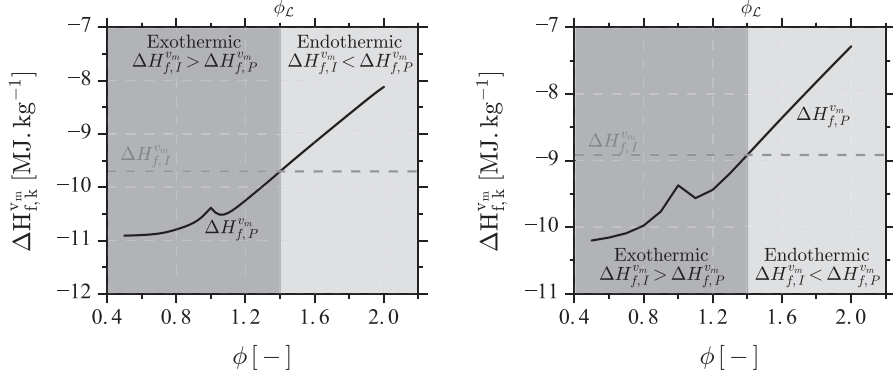
(a) *Methane/air mixture at fresh gas temperature $T_f = 300$ K and pressure $P = 1$ atm*

(b) *Kerosene/air mixture at fresh gas temperature $T_f \approx 700$ K and pressure $P \approx 10$ bar*

Fig. 4. Evolution of the standard enthalpy of formation of the burnt gases virtual mixture with the equivalence ratio. The dotted grey line represents the standard enthalpy of formation of the virtual intermediate species I.

Fresh gases specific gas constant is naturally obtained by assigning real properties to the reactant subset of species A:

$$r_A^{v_m} = r_A^d \quad \text{for } A = \{F, Ox, D\} \tag{27}$$

Virtual product specific gas constant $r_{P_k}^v$ are determined by minimizing the cost function $\mathcal{E}_{\text{chemistry}}^{\text{main}}$ given by:

$$\mathcal{E}_{\text{chemistry}}^{\text{main}}\left(r_{P_k}^{v_m}\right) = \sum_{i=1}^{N_c} \left[\sum_{k \in A} r_k^{v_m} \alpha_{P_k}^{v_m} Y_P^{v_m}|^{eq}(\phi_i) + \sum_{k=1}^{N_p^{v_m}} r_{P_k}^{v_m} Y_{P_k}^{v_m}|^{eq}(\phi_i) \right.$$
$$\left. - \sum_{k=1}^{N_s^d} r_k^d Y_k^d|^{eq}(\phi_i) \right] \tag{28}$$

Transport properties: Virtual mixture-averaged transport properties are closed with simplified models based on analytic laws and dimensionless transport numbers. The mean dynamic viscosity μ^v is given by $\mu^v = \mu_0^v (T/T_0)^{\beta^v}$, where μ_0^v is the dynamic viscosity of the burnt gases in a stoichiometric premixed flame at the reference temperature T_0. The coefficient β^v is optimized to retrieve the viscosity dependence on temperature. The gas mixture thermal conductivity λ^v reads: $\lambda^v = \left(\mu^v c_p^v\right)/\text{Pr}_0^v$, where Pr_0^v is the Prandtl number, assumed constant and equal to the Prandtl number in the burnt gases of a premixed flame at stoichiometry. The molecular diffusion velocities $V_{k,i}^v$ are closed using a unity Lewis number assumption:

$$Y_k^{v_m} V_{k,i}^{v_m} = -D^v \partial_{x_i} Y_k^{v_m} = -\left(\lambda^v/\rho^v c_p^v\right) \partial_{x_i} Y_k^{v_m} \tag{29}$$

In this article, molecular diffusion coefficients D^v of virtual species are assumed equal. It is well established that the use of such simplified transport model impacts both global flame properties [42] and the inner flame structure [43]. However, as it will be discussed in Section 3.1.1, this assumption does not limit the prediction of the laminar flame consumption speed and premixed temperature profiles, as long as targeted flame solutions used to calibrate the main virtual scheme include differential diffusion effects. Nevertheless, to handle changes in elemental composition and displacement of equilibrium properties induced by preferential diffusion, as observed experimentally in [44], transport coefficients of virtual species should be included in the optimization procedure.

2.3.4. Optimization of virtual reaction rate parameters

During the second step of the main virtual mechanism generation procedure (Fig. 3), the kinetic rate parameters are optimized so that the virtual optimized scheme reproduces as best as possible a set of flame properties characterizing the coupling between the flame and the flow field. Here the target quantities retained for the optimization are the laminar flame consumption speed and temperature profiles of 1-D premixed flames.

Chemical reaction rates are expressed with Arrhenius type laws. Rates of progress q_1 and q_2 of reactions R1 and R2 are given by:

$$q_1 = A_1^v f_1^v(Z) \exp\left(\frac{-E_{a,1}^v}{RT}\right) \left([F]^{v_m}\right)^{F_{F,1}^v} \left([Ox]^{v_m}\right)^{F_{Ox,1}^v}, \tag{30}$$

$$q_2 = A_2^v \exp\left(\frac{-E_{a,2}^v}{RT}\right) \left([I]^{v_m}\right)^{F_{I,2}^v f_2^v(Z)}, \tag{31}$$

where A_r^v and $E_{a,r}^v$ are the pre-exponential factor and activation energy of the rth reaction. The exponent $F_{k,r}^v$ corresponds to the forward reaction order of the species k in reaction r. The quantity $[\mathcal{V}_k]^{v_m}$ refers to the molar concentration of the virtual species k. Functions $f_r^v(Z)$ are correction functions dependent on the mixture fraction Z characterizing the fresh gases composition. As unity Lewis numbers are considered here, the mixture fraction is directly related to the normalized dilutant mass fraction, $Z = (Y_D^{v_m} - Y_D^{v_m}|^{Ox})/(Y_D^{v_m}|^F - Y_D^{v_m}|^{Ox})$, where the superscripts F and Ox denote conditions in the pure oxidizer and pure fuel respectively. As suggested by Liñán and Williams, [45], the pre-exponential factor of the first reaction A_1^v is modified by a mixture fraction dependent function f_1^v so as to match the laminar flame speed within the flammability limits. Also, the reaction exponent of the intermediate $F_{I,2}^v$ is corrected by a mixture fraction dependent function f_2^v to control the thickness of the post-flame zone and to improve the flame structure prediction [29].

The genetic algorithm used to optimize species properties is employed to determine the set of reaction rate parameters $(A_r^v, E_{a,r}^v, F_{k,r}^v)$ and correction functions f_1^v and f_2^v that best reproduce the temperature profiles and laminar flame speed. The fitness function $\mathcal{E}_{\text{kinetic}}^{\text{main}}$ comparing solutions obtained using the virtual mechanism and the reference flamelet is defined by:

$$\mathcal{E}_{\text{kinetic}}^{\text{main}}\left(A_r^v, E_{a,r}^v, F_{k,r}^v, f_r^v(Z_i)\right)$$
$$= \sum_{i=1}^{N_c} w_{S_L} \frac{|S_{L_i}^v - S_{L_i}^d|}{S_{L_i}^d} + w_T \frac{\|T_i^v(x) - T_i^d(x)\|_{L_2}}{\|T_i^d(x)\|_{L_2}}, \tag{32}$$

where S_{L_i} and $T_i(x)$, respectively, represent the laminar flame speed and the temperature profile of the ith set of operating conditions ϕ_i. The factors w_{S_L} and w_T are weights attributed to each objective to give appropriate influence to each targeted quantity. For the considered 1-D computational domain and mesh, the values $w_{S_L} = 0.01$ and $w_T = 0.99$ were found to give approximately the

same weight to the laminar flame speed and temperature profile objective.

2.4. Virtual sub-mechanism for minor species prediction

As indicated previously, pollutants are predicted by specific sub-schemes. Virtual sub-mechanisms do not retro-act on the flow field (see equation systems (3) and (4)), but use quantities predicted by the main virtual mechanism. Similarly to the optimization of the main virtual mechanism for temperature prediction, the sub-mechanisms are optimized to capture profiles of a given minor species.
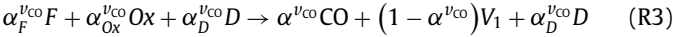
The calibration process aims at evaluating both:

- the minimum number of species and reactions constituting the virtual sub-scheme,
- the best set of kinetic rate parameters so as to reproduce the minor species concentration on the collection of targeted flame configurations.

In this work, the concept of sub-mechanism is applied for the description of CO, but the methodology can be transposed to any minor species.

2.4.1. Optimization of the virtual reaction sub-mechanism for CO

In hydrocarbon/air flames, the CO features an intermediate-like behavior with two characteristic times. In the fuel oxidation layer, CO is rapidly produced through reactions promoted by highly active radicals. Then in the post-flame zone, CO slowly recombines into CO_2. In the virtual chemistry framework, the following set of global reactions is proposed to describe these processes:

$$\alpha_F^{\nu_{CO}} F + \alpha_{Ox}^{\nu_{CO}} Ox + \alpha_D^{\nu_{CO}} D \rightarrow \alpha^{\nu_{CO}} CO + \left(1 - \alpha^{\nu_{CO}}\right) V_1 + \alpha_D^{\nu_{CO}} D \quad (R3)$$

$$F + V_1 \rightarrow F + CO \quad (R4)$$

$$CO \leftrightarrow V_2 \quad (R5)$$

where F, Ox and D are the fuel, oxidizer and dilutant transported in the main mechanism while V_1 and V_2 are virtual species. The first reaction R3 describes the fast CO production from fuel oxidation. The second reaction converting V_1 into CO mimics the slow CO formation processes occurring in rich conditions. Finally, the reversible reaction R5 between CO and V_2 models the slow recombination processes observed in the post-flame zone.

The rate of progress of the virtual reactions R3–R5 are closed with Arrhenius type laws:

$$q_3 = A_3^\nu f_3^\nu(Z) \exp\left(\frac{-E_{a,3}^\nu}{RT}\right) \left([F]^{\nu_{CO}}\right)^{F_{F,3}^\nu} \left([Ox]^{\nu_{CO}}\right)^{F_{Ox,3}^\nu} \quad (33)$$

$$q_4 = A_4^\nu f_4^\nu(Z) \exp\left(\frac{-E_{a,4}^\nu}{RT}\right) \left([F]^{\nu_{CO}}\right)^{F_{F,4}^\nu} \left([V_1]^{\nu_{CO}}\right)^{F_{V_1,4}^\nu} \quad (34)$$

$$q_5 = A_5^\nu f_5^\nu(Z) \exp\left(\frac{-E_{a,5}^\nu}{RT}\right) \left(\left([CO]^{\nu_{CO}}\right)^{F_{CO,5}^\nu} \left([V_2]^{\nu_{CO}}\right)^{F_{V_2,5}^\nu}\right.$$

$$\left. - \frac{\left([CO]^{\nu_{CO}}\right)^{R_{CO,5}^\nu} \left([V_2]^{\nu_{CO}}\right)^{R_{V_2,5}^\nu}}{K_{c,5}^\nu}\right) \quad (35)$$

where $F_{k,r}^\nu$ and $R_{k,r}^\nu$ are, respectively, the forward and reverse reaction orders of the species k in the reaction r. Functions $f_r^\nu(Z)$ are correction functions applied to the pre-exponential factors to improve the predictive capabilities of the virtual sub-mechanism on the whole flammability range. Details about these functions are given in the next session. The closure of the equilibrium constant $K_{c,5}^\nu$ of the reversible reaction R5 is presented hereinafter.

To decrease the computational cost related to the integration of the CO sub-scheme, the species F, Ox and D intervening in reaction R3 are not transported. Instead, we assume that:

$$Y_A^{\nu_{CO}} = Y_A^{\nu_m} \quad \text{for } A = \{F, Ox, D\} \quad (36)$$

This assumption is realized only if the kinetic rate parameters defining the reaction rate of reaction R3 are identical to these of the fuel consumption reaction R1 in the main virtual scheme i.e. if $A_3^\nu = A_1^\nu$, $f_3^\nu = f_1^\nu$, $E_{a,3}^\nu = E_{a,1}^\nu$, $F_{F,3}^\nu = F_{F,1}^\nu$ and $F_{Ox,3}^\nu = F_{Ox,1}^\nu$. Thus, the coefficients A_3^ν, f_3^ν, $E_{a,3}^\nu$, $F_{F,3}^\nu$ and $F_{Ox,3}^\nu$ are not calibrated but their values are fixed by the optimization of the main mechanism. Imposing the kinetic rate parameters of reaction R3 tends to constrain the optimization problem. Typically, the set of kinetic coefficients of reactions R4 and R5 leading to calculation convergence evolve in a reduced domain. This restriction of the parameter domain evolution may lead the calibration procedure to converge towards unwanted kinetic parameters values such as negative reaction orders.

Prediction of the equilibrium state: The equilibrium constant in concentration unit of the rth reaction is given by:

$$K_{c,r}^{\nu_{CO}} = \prod_{k=1}^{N_s^{\nu_{CO}}} \left([X_k]^{\nu_{CO}}|^{eq}\right)^{\alpha_{k,r}^{\nu_{CO}}} \quad (37)$$

For the reverse reaction R5, the equilibrium constant $K_{c,5}^{\nu_{CO}}$ reads:

$$K_{c,5}^{\nu_{CO}} = \frac{[V_2]^{\nu_{s_{CO}}}|^{eq}}{[CO]^{\nu_{s_{CO}}}|^{eq}} \quad (38)$$

Although sub-mechanisms are not involved in mass balance conservation equation, the satellite schemes are built so that the sum of virtual species mass fractions equals one. For the nth sub-mechanism the condition gives:

$$\sum_{k=1}^{N_s^{\nu_{sn}}} Y_k^{\nu_{sn}} = 1 \quad (39)$$

Considering that the virtual species V_1 is completely consumed through reaction R4, and as species F, Ox in reaction R3 are the same as in reaction R1 the equilibrium mass fraction of the virtual species V_2 expresses as:

$$Y_{V_2}^{\nu_{CO}}|^{eq} = 1 - \left(\sum_{k \in A} Y_k^{\nu_m}|^{eq} + Y_{CO}^d|^{eq}\right) \quad (40)$$

where the equilibrium composition of reactants F, Ox and dilutant species D are determined by the main mechanism, while the equilibrium mass fraction of CO is the reference quantity given by complex thermo-equilibrium calculations.

The equilibrium constant $K_{c,5}^{\nu_{CO}}$ is pre-tabulated versus the mixture fraction Z to properly describe the equilibrium state within the flammability limits:

$$K_{c,5}^{\nu_{CO}}(Z) = \frac{[V_2]^{\nu_{CO}}|^{eq}(Z)}{[CO]^d|^{eq}(Z)} \quad (41)$$

As for the main virtual kinetic scheme, the reaction orders are included in the set of optimized parameters to increase the degrees of freedom and enhance the predictivity of the virtual scheme. However, the modification of the reaction orders of the reversible reaction R5 must be consistent with the rule conditioning the chemical equilibrium. In fact, elementary kinetics ensures that the reaction rate of reaction R5 vanishes at equilibrium $q_5|^{eq} = 0$. This condition is expressed using Eqs. (35) and (38) as:

$$\left([CO]^{\nu_{CO}}|^{eq}\right)^{F_{CO,5}^\nu} \left([V_2]^{\nu_{CO}}|^{eq}\right)^{F_{V_2,5}^\nu} = \frac{\left([CO]^{\nu_{CO}}|^{eq}\right)^{R_{CO,5}^\nu} \left([V_2]^{\nu_{CO}}|^{eq}\right)^{R_{V_2,5}^\nu}}{\left([CO]^{\nu_{CO}}|^{eq}\right)^{-1} [V_2]^{\nu_{CO}}|^{eq}} \quad (42)$$
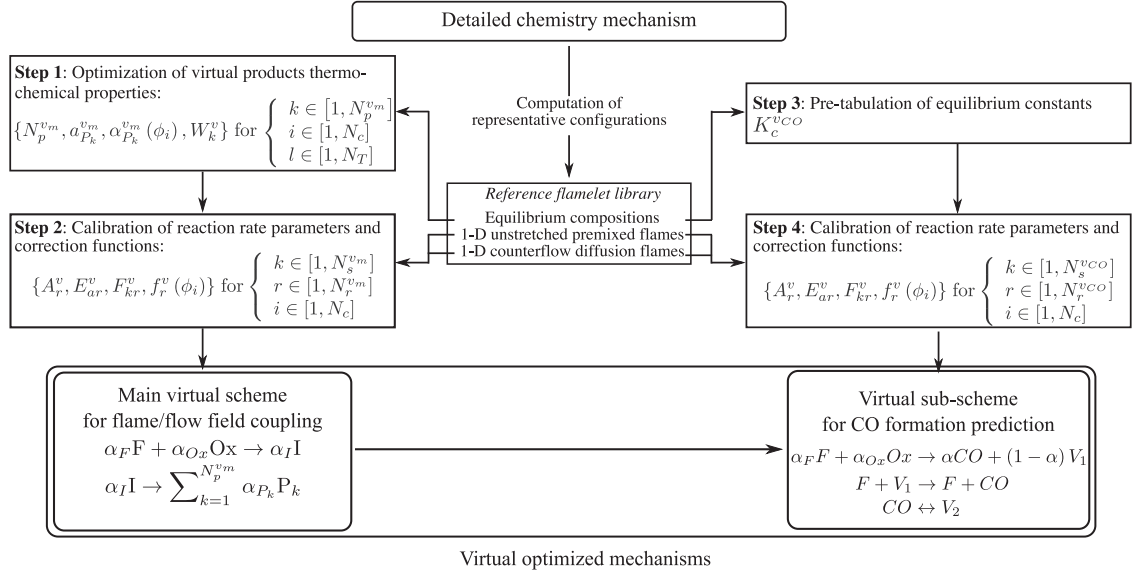
Fig. 5. Summary of the procedure to build virtual optimized mechanisms.

The equilibrium behavior is retrieved if the following conditions are satisfied:

$$F_{CO,5}^v - R_{CO,5}^v = 1 \qquad \text{and} \qquad F_{V_2,5}^v - R_{V_2,5}^v = -1 \qquad (43)$$

Prediction of the CO mass fraction profiles: The virtual sub-scheme is designed so that enough flexibility is given to capture a large variety of CO evolutions. For instance, to match the CO mass fraction peak evolution with the equivalence ratio, the pre-exponential factor A_5^v of reaction R5 is adjusted through a correction function $f_5^v(Z)$ tabulated as function of the mixture fraction Z. In addition, for very rich conditions, detailed chemistry calculations show that CO produced by the combustion of classical hydrocarbon fuels features a slow increase in the oxidation layer. At the opposite for lean and moderately rich mixtures, CO mass fraction profiles exhibit a decrease or constant evolution in the post-flame zone. To account for the different CO mass fraction behaviors in the post-flame zone, the stoichiometric coefficient $\alpha^{v_{CO}}$ of reaction R3 is tabulated versus the fresh gas equivalence ratio. For lean and moderately rich mixtures, $\alpha^{v_{CO}}(Z)$ is set to unity so that CO is first rapidly produced in the reaction zone and then slowly converted into V_2 in the post-flame zone through the equilibrium reaction R5. For rich injection conditions, $\alpha^{v_{CO}}(Z)$ is set lower than unity to model the slow production of CO in the post-flame zone, through reaction R4. Finally, to fit the thickness of the CO oxidation layer, a correction function f_4^v depending on the mixture fraction is applied on the pre-exponential factor A_4^v of reaction R4.

The set of reaction rate parameters and tabulated functions are identified using the optimization algorithm previously introduced. The fitness function $\mathcal{E}_{kinetic}^{CO}$ minimized through the genetic optimization procedure is given by:

$$\mathcal{E}_{kinetic}^{CO}\left(A_r^v, E_{a,r}^v, F_{k,r}^v, f_r^v(Z_i)\right) = \sum_{i=1}^{N_c} \frac{\|Y_{CO_i}^v(x) - Y_{CO_i}^d(x)\|_{L_2}}{\|Y_{CO_i}^d(x)\|_{L_2}} \qquad (44)$$

2.5. Summary

A summary of the different stages for the design of the main and satellite sub-mechanisms is illustrated in Fig. 5. For each step of the virtual mechanisms generation process, the set of unknown parameters or chromosome that must be calibrated are also provided.

3. Application to 1-D laminar methane/air flames

In this section, the strategy presented in Section 2 is applied to the description of the flame/flow field interactions and CO formation in methane/air flames. As described in Fig. 5, a prerequisite to the optimization procedure is the generation of a flamelet library that serves as a reference for the evaluation of the virtual scheme predictive capabilities. The target database, used for the methane/air virtual scheme optimization, is composed by flamelets computed with the detailed chemistry mechanism GRI3.0 [46] and with mixture-averaged transport models [47]. The influence of the flamelet archetypes retained to generate the reference database will be discussed in Sections 3.1 and 3.2.

The performances of the virtual schemes in terms of prediction, computational cost and chemical stiffness are compared against analytically-reduced chemistry, a semi-global mechanism and a premixed-based tabulated chemistry strategy. Table 1 summarizes the chemical models considered for the comparative study.

3.1. Main virtual mechanism

Identification of the fittest reaction rate parameters and correction functions closing the main virtual mechanism is performed with the in-house genetic code described in Section 2.2. The target reference database, used to calibrate the unknown parameters, is made up with $N_c = 31$ one-dimensional unstretched premixed flamelets with fresh gas equivalence ratio varying from lean (ϕ_L=0.5) to rich (ϕ_R=2.0) flammability limits.

3.1.1. Unstretched laminar premixed flames
A series of 1-D laminar freely-propagating premixed methane–air flames is simulated with the chemical combustion models

Table 1
Chemistry description approaches considered for the comparative study.

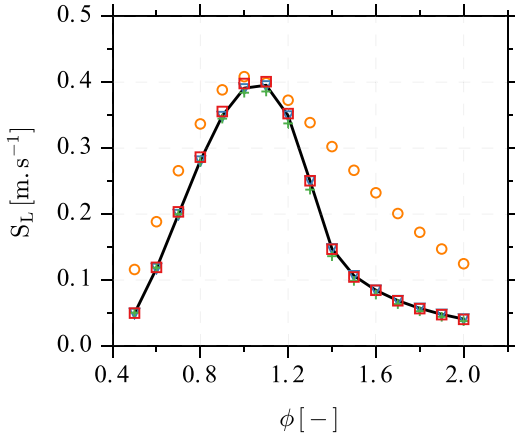| Case	Chemistry description strategy
Reference	Detailed chemistry GRI3.0 [46]
Semi-global	Semi-global scheme Jones [20]
Analytic	Analytically-reduced chemistry LU19 [16]
Tabulated	Premixed based tabulated chemistry FPI [4]
Virtual	Virtual optimized chemistry

Fig. 6. Evolution of the laminar flame speed S_L with the equivalence ratio for a premixed methane/air flame at fresh gas temperature $T_f = 300$ K and pressure $P = 1$ atm. Legend: (——) GRI3.0 reference chemistry, (○) Jones semi-global scheme, (+) LU19 analytic scheme, (▽) FPI tabulated chemistry, (□) Main virtual scheme.

shown in Table 1. Predicted laminar consumptions speeds S_L are plotted in Fig. 6. Except for the Jones semi-global mechanism, the overall agreement between all reduced chemistry approaches and the reference model is good on the whole range of equivalence ratio. The optimized main virtual scheme reproduces well the laminar flame speed in comparison with the detailed mechanism. The optimization of the correction function applied on the pre-exponential factor enables a good agreement between the flame speed evaluated from the low order mechanism and the reference detailed chemistry solutions. Interestingly, as long as the main virtual scheme is trained to reproduce a reference database including differential diffusion effects, the molecular diffusive fluxes may be modeled with a unity Lewis number assumption without impacting the capture of the laminar speed. The tabulated chemistry approach with correction of differential diffusion effects matches very well the reference curve. Finally, the analytically-reduced chemistry method recovers successfully the evolution of the laminar consumption speed.

Figure 7 shows the temperature profiles of a selection of 1-D laminar premixed methane/air flames. For all fresh gas equivalence ratios, the temperature predicted by the main virtual mechanism agrees very well with the detailed reference scheme. The tabulation of the intermediate reaction order $F_{I,2}$ with the mixture fraction enables the adjustment of the characteristic thickness of the post-flame zone and a proper description of the temperature profiles. Also it is worth noting that for very rich condition, at $\phi = 1.8$, the two-step virtual mechanism recovers the temperature decrease from its maximum value to the equilibrium temperature T_{ad} (see inset Fig. 7 bottom right). For this equivalence ratio, the endothermic behavior of reaction R2 allows the temperature reduction in the post-flame zone. Regarding semi-global chemistry, the Jones scheme fails to retrieve the local flame temperature and predicts a very rapid reach of the equilibrium. For all equivalence ratios investigated, the semi-global mechanism shows a very thin post-flame region where the temperature is overestimated. Finally, the analytic mechanism and the tabulated chemistry strategy provide a correct description of the temperature profiles for all equivalence ratios.

3.1.2. Non-premixed counterflow laminar flames

The main virtual mechanism trained to capture the premixed flame structure is *a posteriori* tested on non-premixed flames. A set of counterflow flames has been simulated for strain rates varying from $a = 15 \text{ s}^{-1}$ to a_c, the strain rate at which the diffusion flame is close to quenching. The dependence of peak temperature with strain rate is presented in Fig. 8. For comparison purposes, the results obtained with the one-step model proposed by Er Raiy et al., [30] are added. Though composed of a unique reaction the virtual kinetic scheme provides a satisfactory description of the peak temperature evolution with strain rates. The two-step virtual mechanism captures well the maximum temperature obtained in diffusion flame fronts. However, a slight overestimation of the extinction strain rate is observed. The detailed kinetic model GRI3.0 predicts extinction of the counter-flow diffusion flame for a strain rate a_c^d of 385 s^{-1}, while with the two-step virtual scheme the diffusion flame front persists up to 535 s^{-1}. In this near-extinction region, one may observe that maximum flame
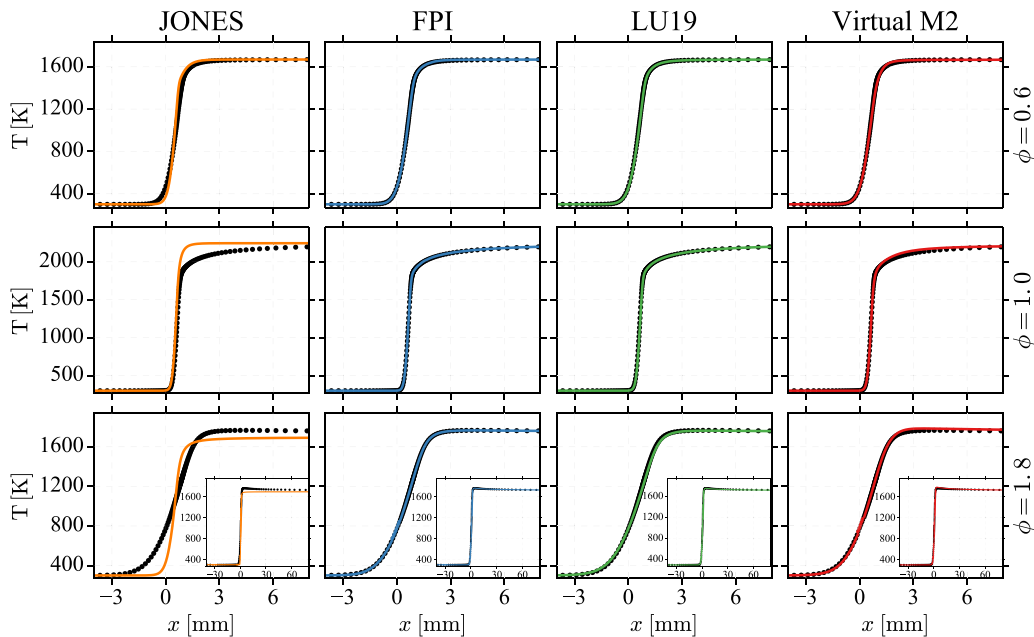

Fig. 7. Spatial evolution of the temperature for premixed methane/air flames at fresh gas temperature $T_f = 300$ K and pressure $P = 1$ atm. Legend: (black dot) GRI.3.0 reference chemistry, (orange line) Jones semi-global scheme, (blue line) FPI tabulated chemistry, (green line) LU19 analytic scheme, (red line) Main virtual scheme.
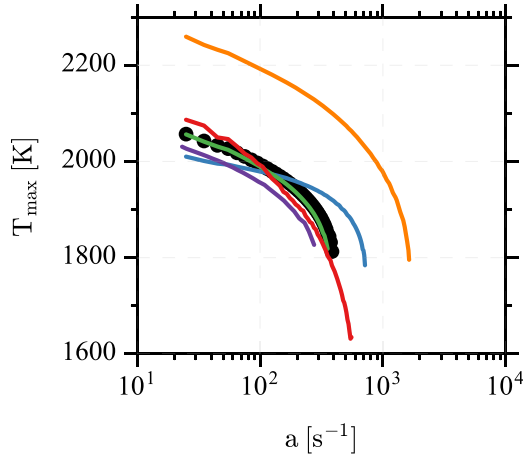
Fig. 8. Evolution with the strain rate of the peak temperature obtained in 1-D counterflow methane/air flames at fresh gas temperature $T_f = 300$ K and pressure $P = 1$ atm. Legend: (● ●) GRI3.0 reference chemistry, (——) Jones semi-global scheme, (——) FPI tabulated chemistry, (——) LU19 analytic scheme, (——) Main virtual scheme, (——) One-step scheme from [30].

temperature predicted by the two-step main virtual scheme are considerably smaller than the reference one. Regarding the semi-global scheme, important overestimation of the peak temperature is noticed for all strain rates. The Jones mechanism is almost not affected by the mechanical effects and overpredicts the quenching strain limit by almost one order of magnitude. The FPI approach tends to underestimates the temperature levels for low strain rates, while over-estimation of the peak temperature is found for high strain rates. The quenching limit predicted by the premixed-based tabulated approach is twice higher than the reference value. Analytically-reduced chemistry reproduces very well the maximum temperature levels and the occurence of flame extinction.

Figure 9 compares spatial temperature profiles predicted by the different kinetic description approaches investigated. Pure methane is injected from the right side and air flows from the left. The temperature profiles predicted by the virtual optimized mechanism match well the reference database for both low and high strain rate conditions (same observations are made for intermediate strain rates). However, the position of the maximum temperature is slightly shifted towards the oxidizer side. As shown in Fig. 8, the semi-global four-step scheme has difficulties to retrieve the impact of strain rate on the counterflow flame structure. The tabulated chemistry strategy provides a reasonable reproduction of
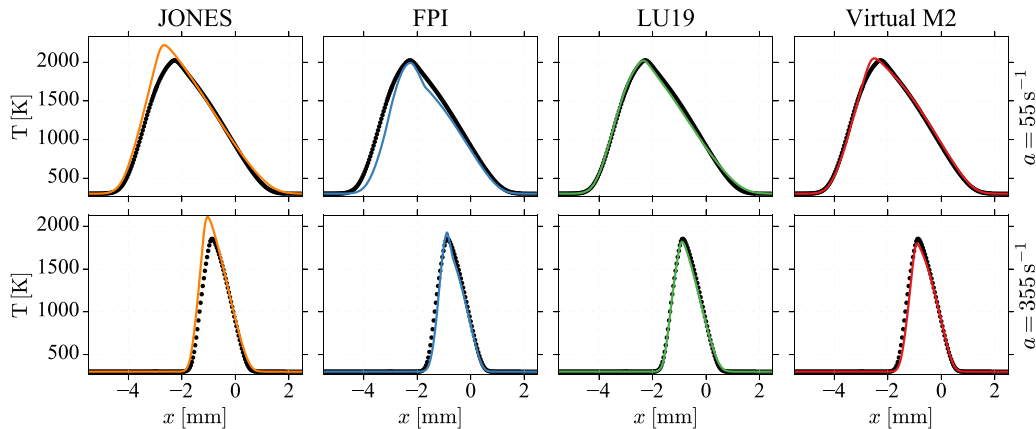
Table 2
Optimization calculations for derivation of the CO sub-mechanisms.

Virtual scheme	Reference database
CO-P	Premixed flames with $\phi = \{0.7, 1.1, 1.6\}$
CO-D	Non-premixed flames with $a = \{50, 150, 250\}$ s^{-1}
CO-P-D	Premixed flames with $\phi = \{1.1, 1.6\}$
	Non-premixed flame with $a = 50$ s^{-1}

the temperature profiles. The temperature departs however from the reference solution in the lean side of the flame. This observation is in accordance with the a posteriori test of the premixed tabulated method on diffusion flames performed in [7]. Eventually, the analytic scheme is in good agreement with detailed chemistry.

3.2. Virtual sub-mechanism for CO formation prediction

The concept of virtual satellite scheme dedicated to the capture of a minor species formation is here tested for CO. The influence of the reference database used to train the virtual mechanism is discussed by calibrating three sub-schemes with three different flamelet library. Table 2 summarizes the different optimization calculations carried out. The first optimization procedure uses a target database composed of a collection of three 1-D premixed laminar flames only, the second reference flame library is made up of three counterflow diffusion reference solutions, while both 1-D premixed and non-premixed laminar flamelets are used in the training database of the third optimization calculation.

3.2.1. Unstretched laminar premixed flames

1-D laminar premixed flames are computed for various equivalence ratios with the different chemistry reduction methods. The ability of reduced chemical schemes to retrieve thermo-chemical equilibrium state is first challenged. For that purpose, compositions of burnt gases is extracted from the steady state solutions of laminar premixed flames.

Figure 10 compares the CO mass fractions in burnt gases of premixed flames predicted by reduced chemistry and detailed mechanism. For the whole range of equivalence ratios, both CO-P and CO-P-D virtual sub-mechanisms reproduce well the equilibrium values thanks to the tabulation of the equilibrium constant in reaction R5. The three other chemistry description strategies, namely semi-global, tabulated and analytic chemistry, also provide a correct description of CO equilibrium mass fractions.

Spatial CO mass fraction profiles predicted by different reduced and tabulated approaches are compared to detailed chemistry solutions in Fig. 11. The virtual optimized sub-schemes trained

Fig. 9. Spatial evolution of the temperature for counterflow methane/air flames at fresh gas temperature $T_f = 300$ K and pressure $P = 1$ atm. Legend: (● ●) GRI3.0 reference chemistry, (——) Jones semi-global scheme, (——) LU19 analytic scheme, (——) FPI tabulated chemistry, (——) Main virtual scheme.
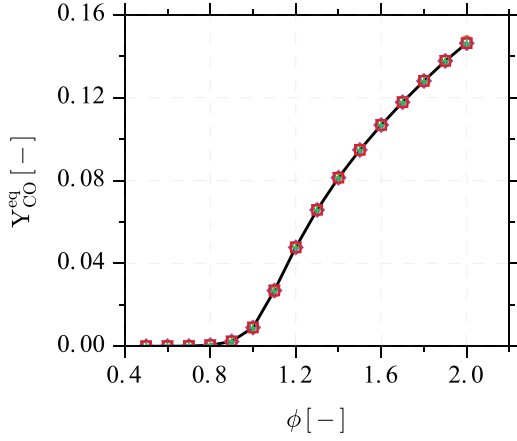
Fig. 10. CO equilibrium mass fraction versus equivalence ratio for premixed methane/air flames at fresh gas temperature $T_f = 300\,K$ and pressure $P = 1\,atm$. Legend: (──) GRI3.0 reference chemistry, (○) Jones semi-global scheme, (+) LU19 analytic scheme, (▽) FPI tabulated chemistry, (□) CO-P virtual sub-scheme, (◇) CO-P-D virtual sub-scheme.

using 1-D premixed laminar flame solutions are in reasonable agreement with detailed chemistry solutions. For lean and stoichiometric injection conditions, the characteristic time to reach the equilibrium value is however either slightly too slow (lean conditions) or too fast (stoichiometry). In rich flames, the optimized virtual sub-mechanisms CO-P and CO-P-D reproduce well the slow increase of CO mass fraction in the post-flame zone. Except in rich conditions, where the CO-P scheme better captures the CO level than the CO-P-D model, the two satellite mechanisms feature similar predictive capabilities with an overall good capture of CO mass fraction profiles. The virtual optimized sub-scheme

derived using non-premixed flames shows reasonably good agreement with the detailed scheme for lean flames. However, as the equivalence ratio increases the deviation between the reference premixed solutions and virtual profiles heightens. In particular, for rich flames, the slow processes of CO production are not accounted for. This observation clearly evidences that the proper description of the CO production in premixed flames is achieved if the virtual sub-scheme is trained using the premixed flame archetype. On the whole range of equivalence ratio investigated, the seven-species semi-global mechanism tends to overestimate the CO mass fraction peaks and predicts a rapid reach to the asymptotic equilibrium value. As expected, the premixed based tabulated strategy FPI and the analytically-reduced mechanism LU19 capture well the CO formation.

3.2.2. Counter-flow diffusion flames

The three virtual sub-mechanisms CO-P, CO-D and CO-P-D are tested on non-premixed flames. Figure 12 compares the CO mass fraction profiles obtained with the different chemistry description strategies of Tables 1 and 2. The Jones semi-global scheme solutions are in overall good agreement with detailed chemistry for all strain rates. Some slight discrepancies with regard to the CO mass fraction peak position and value are however noticeable. Regarding results obtained using the analytically-reduced mechanism, Fig. 12 shows that a very good agreement is obtained for the all range of strain rates investigated. The virtual satellite scheme calibrated to capture CO in counter-flow diffusion flames matches well the flame solutions evaluated with the reference detailed scheme GRI3.0. If the two virtual blocks CO-P and CO-P-D give similar responses in premixed configurations, this is not the case in non-premixed mode. For low strain rates, CO-P sub-mechanism built from a premixed database highly overestimates the CO levels. On the contrary, the mass fraction profiles are well captured with the CO-P-D virtual scheme for low strain rates. The addition of
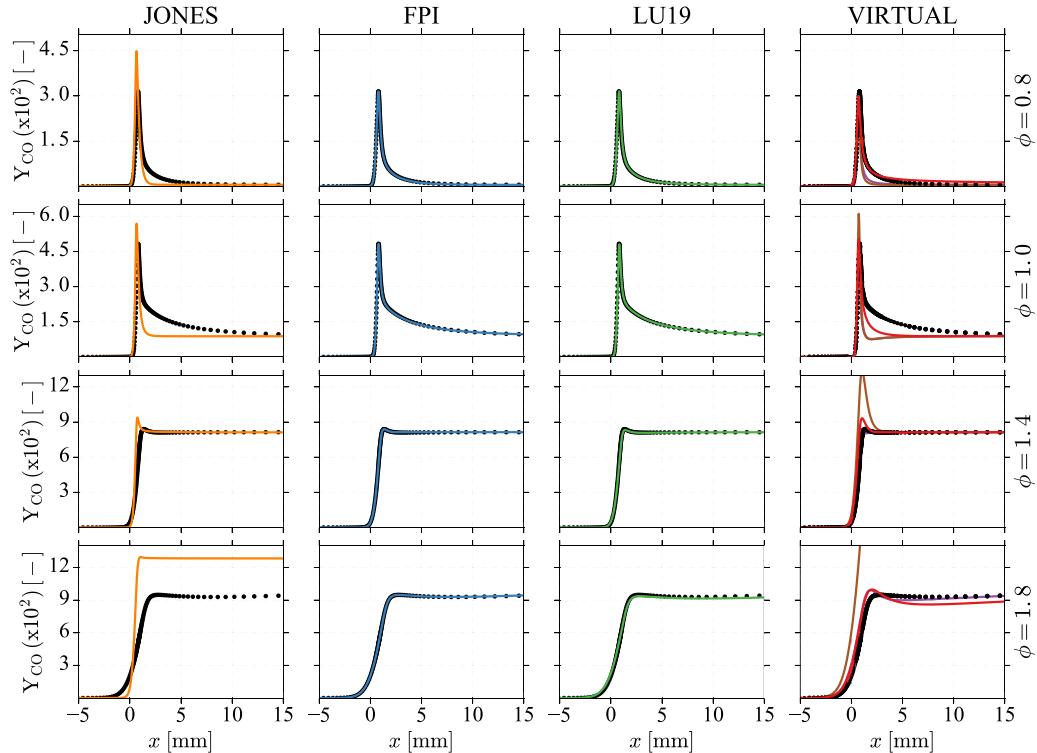

Fig. 11. Spatial evolution of the CO mass fraction Y_{CO} for a 1-D premixed methane/air flame at fresh gas temperature $T_f = 300\,K$ and pressure $P = 1\,atm$. Legend: (● ●) GRI3.0 reference chemistry, (──) Jones semi-global scheme, (──) LU19 analytic scheme, (──) FPI tabulated chemistry, (──) CO-P virtual sub-scheme, (──) CO-D virtual sub-scheme, (──) CO-P-D virtual sub-scheme.
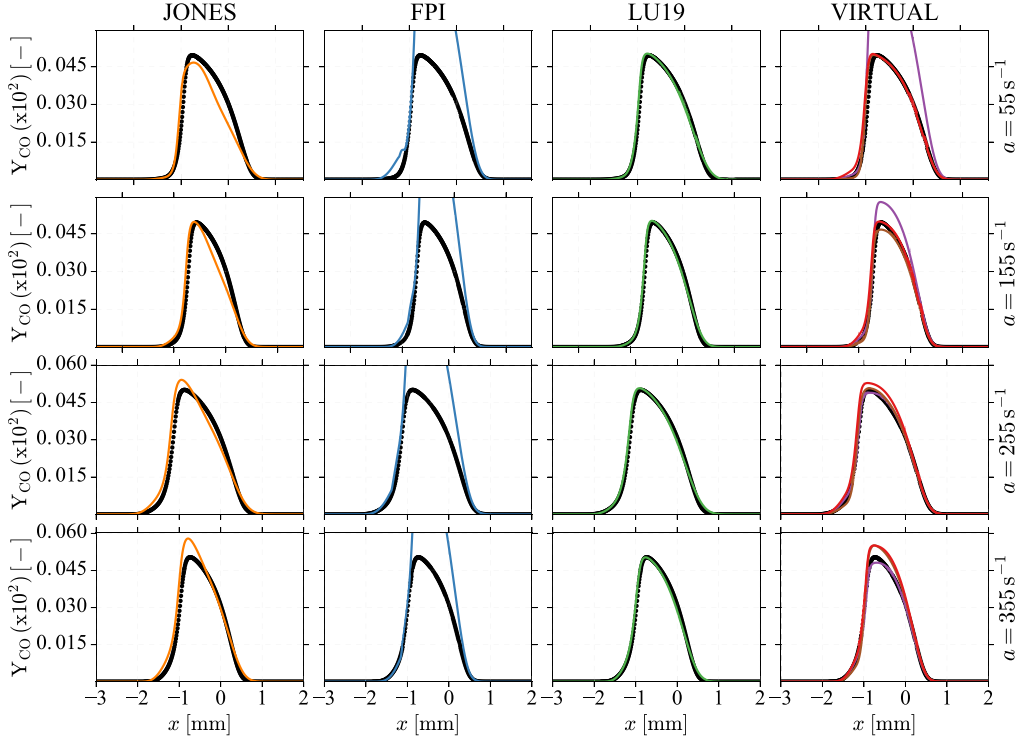
Fig. 12. Spatial evolution of the CO mass fraction Y_{CO} for 1-D counterflow methane/air flames at fresh gas temperature $T_f = 300$ K and pressure $P = 1$ atm. Legend: (● ●) GRI3.0 reference chemistry, (——) Jones semi-global scheme, (——) LU19 analytic scheme, (——) FPI tabulated chemistry, (——) CO-P virtual sub-scheme, (——) CO-D virtual sub-scheme, (——) CO-P-D virtual sub-scheme.

Table 3
Averaged relative errors of chemical strategies compared to virtual chemistry approach for 1-D premixed and diffusion flame calculations with REGATH.

Case	Premixed flames				Diffusion flames		
	$\mathcal{E}_{S_L}$[%]	$\mathcal{E}_T$[%]	$\mathcal{E}_\rho$[%]	$\mathcal{E}_{CO}$[%]	$\mathcal{E}_T$[%]	$\mathcal{E}_\rho$[%]	$\mathcal{E}_{CO}$[%]
Jones semi-global	77.95	0.43	0.55	8.70	11.44	2.26	16.24
LU19 analytic	4.38	0.16	0.08	0.89	2.59	0.71	5.78
FPI tabulated	0.19	0.03	0.04	0.35	8.58	3.42	84.81
M & CO-P virtual	1.11	0.15	0.10	5.07	5.65	1.96	23.00
M & CO-D virtual	1.11	0.15	0.10	6.92	5.65	1.96	7.32
M & CO-P-D virtual	1.11	0.15	0.10	5.91	5.65	1.96	11.75

the non-premixed strained flame archetype at $a = 50$ s^{-1} in the reference library greatly improves the predictive capabilities not only for $a = 55$ s^{-1} but also for higher strain rates. Near extinction, it may however be noticed that the virtual sub-scheme built to capture CO in premixed flames better capture the CO mass fraction peak than the CO-P-D virtual mechanism. As shown in Table 3, the global error associated with the CO-P-D virtual satellite scheme is importantly reduced in comparison with the CO-P sub-mechanism. Therefore to properly predict CO levels the kinetic model must be optimized on both premixed and non-premixed flame. This conclusion is consistent with tabulated chemistry solutions, where the premixed-based tabulated approach does not capture the CO profiles. Unlike heat release and temperature, it appears mandatory to account for the co-existence of different combustion regimes to capture pollutant species such as CO.

3.3. Overall model errors for both premixed and non-premixed flames

The deviation between reduced chemistry models and the reference complex kinetic scheme is quantified by adding error criteria for each quantity of interest. The averaged relative error between the reduced model r and the detailed model d associated with the target quantity s is given by:

$$\mathcal{E}_s = \frac{1}{N_{op}} \sum_{i=1}^{N_{op}} \frac{\|s_i^r(x) - s_i^d(x)\|_{L_2}}{\|s_i^d(x)\|_{L_2}} \quad (45)$$

where N_{op} is the number of operating conditions tested (i.e. equivalence ratio for premixed flames or strain rates for diffusion flames).

Table 3 summarizes the mean level of errors for both premixed and non-premixed flames. Relative errors for the quantities considered during the optimization procedure (laminar flame speed $\mathcal{E}_{S_L}$, temperature $\mathcal{E}_T$ and CO mass fraction $\mathcal{E}_{CO}$) are presented. The relative error norms associated with the capture of density profiles ($\mathcal{E}_\rho$), which are not explicitly targeted when deriving the virtual mechanism, are also given. As expected, in premixed combustion mode, the FPI tabulated chemistry approach yields negligible error levels (lower than 1%) mainly associated with the choice of the progress variable. However, as noticed in Fig. 12 when the premixed tabulated method is used to simulate counterflow non-premixed flame configurations, it fails to capture CO concentration levels. Regarding analytically-reduced chemistry scheme, small de-

Table 4

Relative and normalized costs of chemical strategies compared to virtual chemistry approach for 1-D premixed flame calculations with REGATH. M stands for the main virtual mechanism.

Case	Transport model	Nb. of eq. N_{eq}	Rel. CPU time $\mathcal{C}_r = T/T^v$	Norm. CPU time $\mathcal{C}_n = (\mathcal{C}_r N_{eq}^{v\,2})/N_{eq}^2$
GRI3.0 reference	Complex	55	135	7.58
Jones semi-global	$Sc_k = cst$	9	0.76	1.57
LU19 analytic	$Sc_k = cst$	21	9.55	3.66
FPI tabulated	$Sc_k = cst$	3	0.07	1.30
M and CO-P-D virtual	$Sc_k = cst$	13	1.00	1.00

viation levels are obtained for both premixed and non-premixed conditions. As analytic schemes are derived retaining important chemical pathways and chemical compounds they also conserve a good physical representation of the chemical phenomena. In premixed combustion mode, the four-step semi-global mechanism features important error levels for all flame variables of interest. These high discrepancies are mainly due to (i) the overestimation of laminar flame speed in rich conditions leading to shorter thermal thicknesses, and (ii) an underestimation of the chemical time scales in the post-flame region leading to temperature and CO mass fraction overpredictions. In non-premixed flame configurations, the Jones kinetic scheme is associated with acceptable error levels for the CO mass fraction prediction, but lacks of predictive capabilities for temperature description compared to other models. In premixed mode, when premixed flames are included in the reference database used to train virtual schemes, the optimized chemistry approach provides acceptable error levels for all quantities investigated. In non-premixed conditions, the main virtual optimized schemes dedicated to the prediction of the flame/flow field coupling produces acceptable overall error levels of about 5%. As regards with CO formation prediction in diffusion flames, the CO-D virtual sub-mechanism associated with the main virtual scheme produces a small deviation of 7.32% in comparison with the detailed GRI mechanism. If the virtual satellite scheme is trained using only 1-D premixed laminar flames the agreement between the reference database and the reduced scheme is considerably reduced leading to an averaged error of 23%. This discrepancy is reduced to 12% with the virtual CO-P-D sub-scheme built using both premixed and non-premixed flames in the learning database.

3.4. Computational costs

The computational time associated with the calculation of a stoichiometric monodimensional laminar premixed flame is discussed. The resolution of such canonical problem is performed with the REGATH flame solver based on a Newton-type algorithm whose cost is mainly dependent on the evaluation of the Jacobian matrix and the inversion of the system. It can be shown that this cost is proportional to the number of reactions and scales with the number of equations to solve squared [48]. When complex transport models are used, a non-negligeable additional cost is associated with the evaluation of binary diffusion coefficients. Finally, the computational cost is also dependent on the stiffness of the numerical system.

Table 4 presents the relative CPU time $\mathcal{C}_r$ of the different chemical strategies with respect to virtual chemistry. The cost of an iteration T is averaged over 50 iterations to ensure representativity of the comparison. The normalized cost $\mathcal{C}_n$, whose definition is given in Table 4, is added to highlight the overcosts associated with transport modeling and chemical stiffness. Compared to the detailed scheme, virtual chemistry allows a reduction of computational time by a factor of 135. As the normalized cost is not close to unity, this high difference is not only due to the size of the kinetic scheme. Indeed, the chemical stiffness of the

detailed mechanism and the complex transport model used to close the molecular diffusive fluxes contribute importantly to the overall cost of the calculation. With identical transport models, the simulation of a 1-D premixed flame using virtual chemistry is about 10 times less expensive than with analytic chemistry. The computational gain offered by virtual mechanisms is first related with the low number of species and reactions involved in the virtual scheme compared with the analytically-reduced model. Secondly, the residual stiffness of the analytic mechanism tends to increase the computational time associated with the resolution of species transport equations (see stiffness analysis hereinafter). Comparing the proposed strategy with semi-global chemistry shows that virtual chemistry is about 25% more expensive. This 25% difference, explained by the additional number of transported species involved in virtual mechanisms, is acceptable. Finally tabulated chemistry strategy is more than ten times cheaper than virtual chemistry. However, as the normalized cost is almost unity, we can conclude that the extra cost associated with virtual chemistry is mainly due to the number of transported variables.

3.5. Stiffness analysis

One key feature of a kinetic scheme is its chemical stiffness. A reactive system of equations is defined as stiff if some components of its solution respond very quickly, while others respond quite slowly [49]. In the combustion chemistry community, stiffness analysis is most often characterized by evaluating the chemical time scales τ_k of all species involved in the kinetic model. These key quantities may be identified through various definitions generally based on the analysis of the linearized system of differential equations [50]. The most refined and computationally demanding method express the chemical time scales as the inverse of the eigenvalues of the Jacobian of the chemical source terms matrix [51,52]. Chemical time scales may also be computed without explicit evaluation of the Jacobian eigenvalues. For example, Løvås et al., [53] defined the species lifetime as the inverse of the diagonal element of the Jacobian matrix. Alternatively, global system progress time scale based on the Jacobian matrix [50] may be used for turbulence-chemistry interaction modeling. In this framework, Caudal et al., [54] introduced a refined eigenvalue time scale definition, called Chemical Time Scales Identification (CTS-ID) method, allowing the identification of relevant time scales by comparing the eigenvectors direction to the chemical system trajectory.

In this work, both the classic eigenvalue time scale and the refined one proposed by Caudal et al., [54] are retained to evaluate the chemical time scales exhibited by the different chemistry description methods. Figure 13 shows the spatial evolution of the chemical time scales across a stoichiometric premixed flame front. Relevant time scales, associated with chemical trajectories contributing for more than 1% of the highest contribution, are displayed with black dots. While non relevant time scales, i.e. not related to the chemical trajectory, are represented with gray dots. As expected, the GRI3.0 detailed kinetic mechanism features a wide range of chemical time scales, that may lead to a
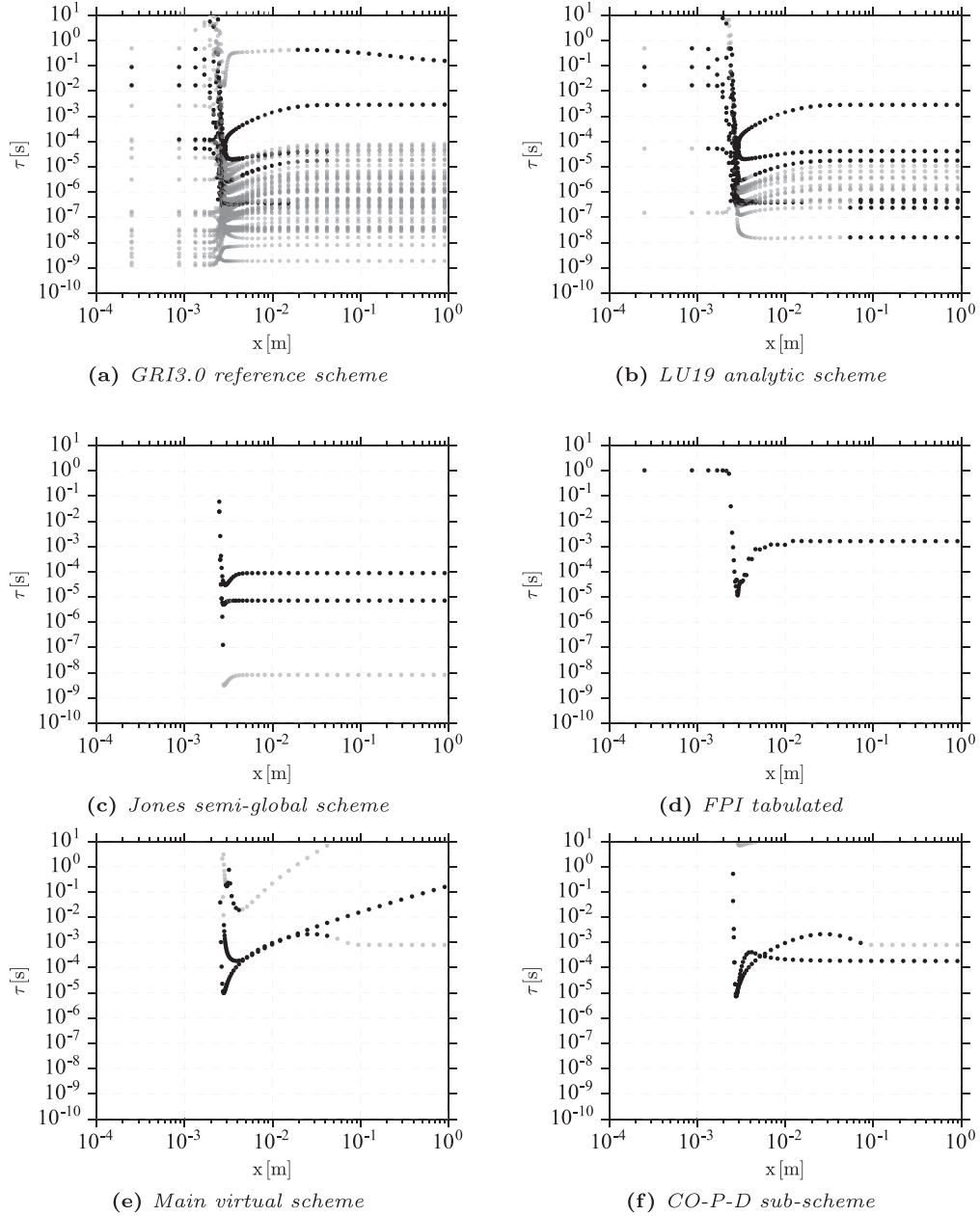
Fig. 13. Chemical time scales for a stoichiometric laminar premixed methane/air flames at fresh gas temperature T_f = 300 K and pressure P = 1 atm. Legend: (black dots) relevant time scales, (gray dots) non-relevant time scales.

very stiff behavior compared to other methods. If only relevant time scales are considered, the smallest contribution is found in the flame front region with a characteristic time scale of about 6.0×10^{-8} s. Regarding analytically-reduced scheme, one may observe that relevant time scales in the highly reactive zone ($x \in \left[10^{-3}, 10^{-2}\right]$ m) range within a shorter interval than with complex detailed chemistry. However, the smallest relevant chemical time scale of 3.0×10^{-7} s is lower than those exhibited with virtual or tabulated chemistry, confirming the hypothesis of residual stiffness. The Jones semi-global mechanism presents smallest relevant chemical time scales ranging between 1.0×10^{-7} and 1.0×10^{-6} s, that are smaller than those obtained with virtual optimized mechanisms. As discussed by Pruefert et al., [50], the chemical time scales evaluated from the source term of the progress variable (i.e. for the premixed tabulated chemistry method) may be interpreted as the overall chemical time scale

of the system, or more precisely, of the main products formation. Interestingly, the chemical time scales of the progress variable are very similar to the chemical time scales of the virtual schemes, meaning that virtual schemes mainly capture the overall dynamic of the chemical system. Moreover, the reduced chemical stiffness exhibited by the virtual chemistry approach constitutes a real advantage regarding the cost of the species transport equation integration.

4. Modeling of 2-D laminar methane/air burners

The virtual optimized mechanisms for CH_4/air combustion have been successfully validated on 1-D premixed and non-premixed flames. The predictive capabilities of virtual chemistry are now assessed on two-dimensional laminar partially-premixed burner. This simple laminar configuration has been chosen for two main
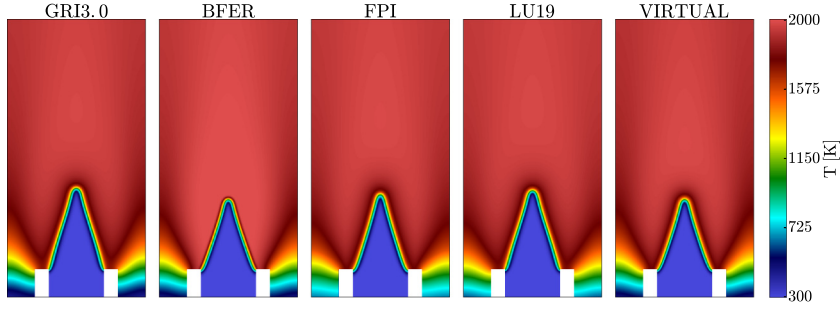
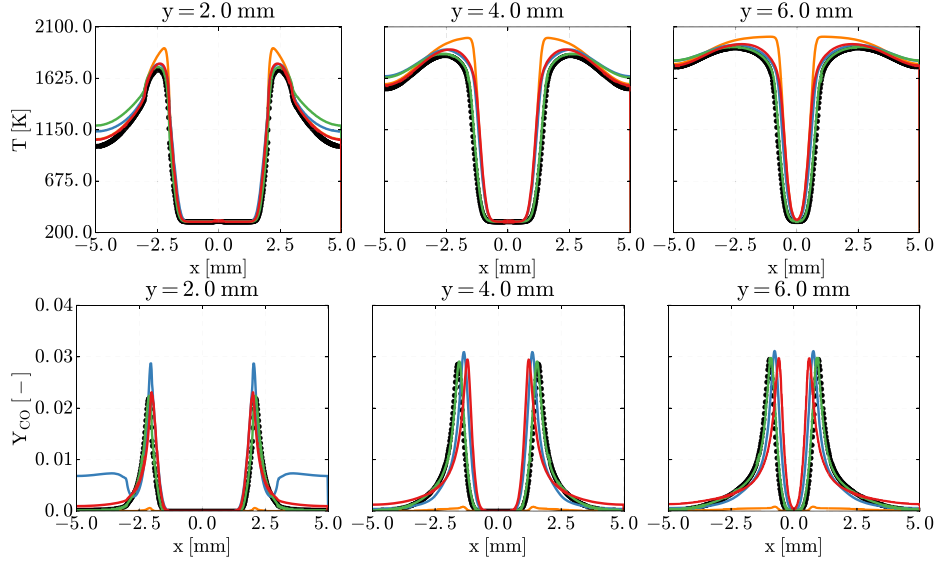**Fig. 14.** Temperature field in the laminar partially premixed burner.

Fig. 15. Horizontal profiles of temperature (top) and CO mass fraction (bottom) for different axial positions. Legends: (● ●) GRI3.0 reference chemistry, (──) BFER semi-global scheme, (──) LU19 analytic scheme, (──) FPI tabulated chemistry and (──) Virtual mechanisms.

reasons. First, laminar flow configuration eliminates the impact of turbulent combustion modeling, enabling a focus on combustion kinetics effects only. Secondly, the small dimensions of the burner make Direct Numerical Simulation accessible in terms of CPU time even with complex chemistry model. The objective is to compare and analyze DNS of a partially-premixed burner performed with the chemistry description strategies investigated in Section 3. The four-step Jones mechanism is however replaced with the two-step semi-global scheme proposed by Franzelli et al., [55].

The 2-D burner studied in this work has been previously investigated by authors in [56,57] in non-adiabatic conditions. The burner geometry and its dimensions are detailed in [57]. A lean methane–air mixture, featuring a fresh gas equivalence of ratio of $\phi_P = 0.8$, is injected through a central injector. The primary stream is surrounded by air co-flow to isolate the flame from ambient perturbations. For both streams, the inlet velocity profile prescribed is a plug flow with characteristic velocity $U_{cf} = 0.05\,\mathrm{m\,s^{-1}}$ for the co-flow, and $U_P = 0.8\,\mathrm{m\,s^{-1}}$ (Re$_P$=125) for the primary inlet. The fresh gases temperature and pressure correspond to atmospheric conditions. As virtual chemistry mechanisms have been built to capture adiabatic flame configurations, injector walls are treated with adiabatic conditions. The transverse size of the computational domain being large enough to avoid interactions between premixed branches and the side boundaries, symmetry boundary conditions are considered for lateral walls. The computational domain is discretized into 1.0 million cells featuring a characteristic size Δ_x of 20 μm. With a laminar flame thickness $\delta_L^0|$ of 0.5 mm, the thermal flame front is resolved on about 25

points. Direct Numerical Simulations have been performed with the low-Mach number, unstructured finite volume flow YALES2 solver [58]. A centered fourth-order scheme is used for spatial discretization, while temporal integration is performed explicitly using a fourth-order TFV4A scheme [59].

Figure 14 displays the temperature fields predicted by detailed, analytic, semi-global, tabulated and virtual chemical models. The direct comparison of the temperature 2-D fields demonstrates a qualitative good agreement between all chemistry modeling approaches. All reduced chemical models provide a good reproduction of the temperature levels. A small difference is however noticeable for the global BFER scheme that over-predicts the temperature in the post-flame zone. The flame lengths comparison shows that the virtual optimized scheme, the semi-global mechanism and the premixed tabulated strategy predict a shorter flame than detailed and analytic chemistry solution. The reasons for these discrepancies may be mainly attributed to transport modeling. Tabulated, semi-global and virtual chemistry approaches close the diffusion fluxes with a unity Lewis number assumption. While, the analytic scheme evaluates species diffusivities assuming a constant Schmidt number for each species. The phenomena combining flame curvature and preferential diffusion effects, occurring in the direction tangential to the flame front, are not properly captured with the simple transport models.

Quantitative comparisons regarding temperature prediction are provided in Fig. 15 (top) where radial profiles of temperature are plotted for different axial distances from the computational domain entrance. The virtual optimized mechanism captures well the

temperature evolution for the three positions investigated. Very good agreement is also observed between detailed, LU19 analytic and premixed-based tabulated models. However, the BFER semi-global scheme is not able to reproduce the temperature evolution in the flame front. The radial profiles of CO mass fraction are displayed in Fig. 15 (bottom). As discussed in [55], the BFER semi-global scheme largely under-predicts the CO concentration in the flame region, whereas premixed-based tabulated approach slightly overestimates it above the burner exit plane. Eventually, both analytically-reduced chemistry and the virtual chemistry approach recover well the detailed solution.

5. Virtual optimized schemes for heavy fuels

This section presents the application of the virtual chemistry approach for the derivation of reduced virtual schemes describing the oxidation of heavier hydrocarbon fuels. Main objective of this part is to demonstrate the relevance of the method independently of the fuel size and complexity. Low temperature and preferential diffusion effects, predominant for heavy hydrocarbon combustion, are not treated in this article.

Four virtual optimized mechanisms dedicated to the prediction of ethylene, propane, heptane and kerosene oxidation are build up by reducing the four detailed chemical mechanisms indicated in Table 5. Despite the various sizes of the reference complex schemes (the number of species ranges from 91 to 297 and the number of elementary reactions varies from 694 to 16,797), all corresponding reduced virtual schemes are composed by the same number of virtual species (11) and virtual reactions (5). Main virtual schemes dedicated to temperature prediction involve 8 species (three reactants, one virtual intermediate species and four virtual products) interacting through two global reactions. Three addi-

tional species and three virtual reactions are required to describe CO formation.

In the following, all reduced virtual schemes are optimized for atmospheric initial conditions, except the kerosene virtual kinetic model which is designed for high pressure and temperature operating point. The reference database used to identify the thermodynamic properties and molecular weights of the virtual product species are composed by $N_c = 31$ constant pressure adiabatic equilibrium calculations, with equivalence ratio varying from lean ($\phi_L = 0.5$) to rich ($\phi_R = 2.0$) flammability limits. The main virtual scheme and the CO satellite mechanism are built up to capture the flame temperature and CO formation in premixed flames computed with the detailed chemistry of Table 5 and with mixture-averaged transport models [47]. Diffusion flames are not included in the target database as preferential diffusion effects, dominant in heavy hydrocarbon/air counterflow flames are not treated at this stage.

Capabilities of the virtual optimized mechanisms to capture global flame properties such as adiabatic flame temperature and laminar flame speed are first assessed. Then, two virtual optimized mechanisms designed to retrieve the flame/flow field coupling and CO formation in kerosene/air flames are evaluated on laminar premixed flames.

5.1. Global flame properties of complex fuels

Figure 16 (left) compares the adiabatic flame temperatures predicted by mixtures composed of four virtual products with optimized thermodynamic properties against reference equilibrium calculations. For each fuel, a very good agreement is obtained between virtual and complex kinetic solutions on the whole range of equivalence ratio. Even for heavy hydrocarbons such as kerosene, only four virtual products are required to describe the equilibrium

Table 5
Hydrocarbons and reference kinetic schemes used to derive reduced virtual main and sub-scheme schemes.

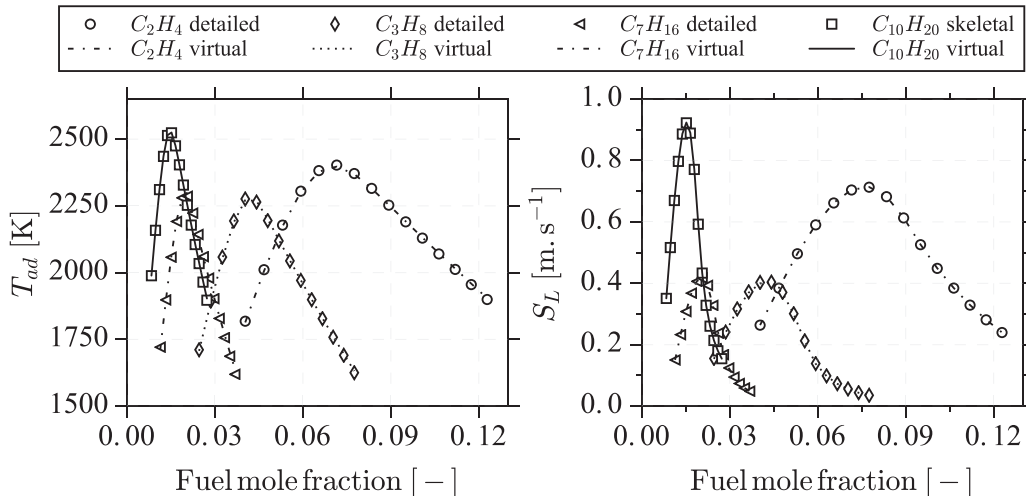| Hydrocarbons	Detailed scheme	Ref.	Virtual main scheme	Virtual CO sub-scheme
Ethylene	297 species	[60]	8 species	3 species
(C_2H_4)	16797 reactions		2 reactions	3 reactions
Propane	111 species	[61]	8 species	3 species
(C_3H_8)	784 reactions		2 reactions	3 reactions
N-heptane	106 species	[62]	8 species	3 species
(C_7H_{16})	1738 reactions		2 reactions	3 reactions
Kerosene surrogate	91 species	[15]	8 species	3 species
($C_{10}H_{20}$) [63]	694 reactions		2 reactions	3 reactions

Fig. 16. Adiabatic flame temperature and laminar flame speed versus fuel mole fraction for hydrocarbon/air mixtures.
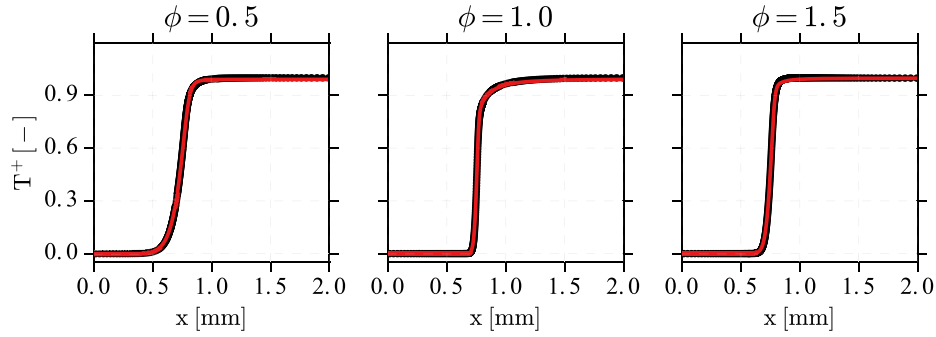
Fig. 17. Spatial evolution of the dimensionless temperature $T^+ = T/T_f$ for premixed kerosene/air flames. Legend: (● ●) Luche reference mechanism and (━) main virtual scheme.
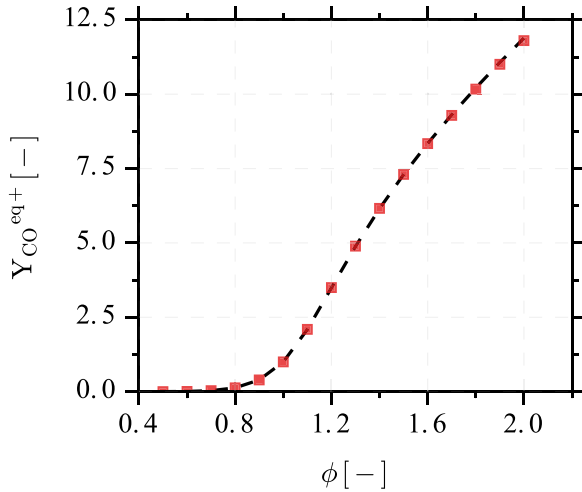

Fig. 18. Dimensionless equilibrium CO mass fraction $Y_{CO}^{eq+} = Y_{CO}^{eq}/Y_{CO}^{eq\,d}|_{st}$ versus equivalence ratio for kerosene/air mixture. Legend: (━━) Luche reference mechanism and (■) CO virtual sub-scheme.

state. The laminar flame speeds are also well captured by the virtual mechanisms over the whole flammability range, as presented in Fig. 16 (right).

5.2. Flame temperature and CO formation in premixed kerosene/air flames

Ability of the virtual two-step mechanism to capture local flame temperature in premixed flame fronts is investigated in Fig. 17. Over the whole flammability range, temperature profiles predicted by the virtual mechanism are in very good agreement with the reference flame solutions. As noticed for methane–air combustion,
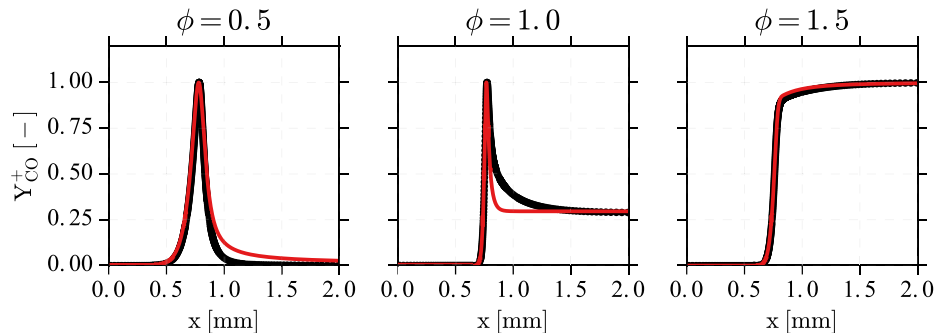
the one-layer thermal flame structure typical of lean conditions and the two-layer thermal flame regime observed in moderately rich injection condition are well recovered by the two-step scheme.

A satellite sub-mechanism dedicated to the capture of CO formation processes is used in combination with the main virtual mechanism. Equilibrium CO mass fractions predicted by the virtual sub-mechanism are compared with reference equilibrium computations performed with the set of 91 species included in the Luche skeletal scheme (Fig. 18). For the whole flammability range, a good agreement is obtained between the virtual optimized model and the reference equilibrium calculations. Figure 19 shows the CO mass fractions profiles predicted by the virtual satellite scheme and the skeletal mechanism. For the three equivalence ratios investigated, an overall good agreement is obtained between the reduced virtual scheme and the detailed one. However, as noticed for near-stoichiometric methane oxidation, the characteristic time to reach the equilibrium is slightly mispredicted.

6. Conclusions and discussions

A reduced-cost chemical modeling strategy, called virtual optimized chemistry, has been proposed. This approach relies on building up virtual optimized schemes that are composed of virtual species and reactions. In this framework, virtual species properties and reaction rate parameters are calibrated to retrieve quantities of interest such as flame temperature and minor species, on a range of selected flame configurations. An automated procedure, based on genetic algorithm, allows to identify (i) the physical properties of virtual species that best describe mixture-averaged properties of a real reference mixture, (ii) the set of kinetic rate coefficients allowing a proper description of a reference database composed by a collection of laminar flamelets. Flame/flow field coupling and minor species formation processes are modeled by different sub-mechanisms.

Fig. 19. Spatial evolution of the dimensionless CO mass fraction $Y_{CO}^+ = Y_{CO}/\max(Y_{CO}^d)$ for premixed kerosene/air flames. Legend: (● ●) Luche reference mechanism and (━) CO virtual sub-scheme.

In this article, the methodology is first illustrated by the derivation of two sub-mechanisms dedicated to the prediction of heat release and CO formation in methane/air flames. The resulting virtual schemes are compared to different chemistry description strategies on 1-D laminar premixed and non-premixed flames. For both targeted quantities and flame archetypes analyzed, virtual chemistry is in good agreement with detailed chemistry, and shows good predictive capabilities in comparison with classical chemistry reduction approaches. The influence of the reference database used to design the virtual mechanism has been studied. It has been shown that contrarily to heat release prediction, CO emissions modeling is impacted by the choice of the reference database used to train the virtual mechanism. When both premixed and non-premixed flame elements are included in the reference flamelet library the predictive capabilities of the virtual sub-mechanism are improved.

The new chemical model has also been used for the generation of virtual schemes devoted to the description of kerosene/air combustion in high pressure and high temperature conditions. While keeping the same mechanism architecture than for methane, the CO concentrations and heat release rate are well captured, suggesting that the size of the reduced virtual scheme does not depend on the number of reactions and species involved in the reference mechanism.

The newly proposed strategy appears as a promising reduced-cost modeling technique to account for chemistry effects. It may for instance be used in combustion chamber design phase stage to efficiently assess the effect of technological changes on CO formation and temperature. Future works intend to challenge this new strategy on other pollutants species such as NO_x and PAH. Though the methodology can theoretically be transposed to any chemical species, difficulties associated with the capture of chemical processes evolving with dramatically different time scales should be addressed. Also, it would be of great interest to test and extend the virtual optimized concept to a wider range of operating conditions (initial pressure and temperature, dilution *etc.*) and flame configurations (auto-ignition problems, cold flames *etc.*). In the present work, the transport properties of the virtual species are closed with simplified models that do not account for preferential diffusion effects. However, in configuration where the flame is not perfectly planar, the combined effects of stretch and preferential diffusion may not be captured. A perspective would be to include the virtual species molecular diffusion coefficients in the set of parameters to optimize and add laminar strained premixed flames in the training database. Finally, to improve the accuracy of the virtual schemes and its range of applicability an automated method to identify the mechanism structure should be developed. For instance, the nature (consecutive, competing, equilibrium) and the number of virtual chemical reactions could be identified by exploiting information contained in reference flame solutions.

As discussed in the introduction, reduced combustion chemistry can be modeled through three routes namely analytic, semi-global and tabulated chemistry.

If analytic chemistry provides a reliable description of complex kinetic effects, the numerical difficulties associated with equations stiffness or its extension to the prediction of heavy molecules such as soot precursors constitute drawbacks compared to virtual chemistry. Additionally, derivation of analytic kinetic schemes describing the combustion of complex and heavy hydrocarbon such as alternative fuels may results in high dimensionality mechanisms.

Semi-global chemistry and optimized virtual strategy present similar computational costs. However, unlike standard semi-global schemes, virtual mechanisms are able to capture quantities of interest, even if related to complex chemistry phenomena. Here, it has been shown that CO mass fraction and complex temperature profiles are reasonably predicted by virtual optimized chemistry.

Finally, even though, tabulated chemistry formalism is cheaper than virtual chemistry, its range of validity is limited to simple flame archetypes. For instance, the comparative study performed in Section 3.2 showed that premixed-based tabulated methods are not able to capture CO formation in non-premixed flame configurations. As discussed in previous works [7,8,64,65] the domain of validity of tabulated chemistry can be extended by adding various flamelet configurations (premixed, partially-premixed and diffusion) in the database and by increasing the number of control parameters. However the tabulation of these different types of flame elements in one unique table raises various problems. Among them we can mention (i) coordinates identification difficulties [66,67], and (ii) theoretical difficulties to close the balance equations in both laminar and turbulent context [2,68]. These different issues limit the practical applicability of tabulated chemistry approaches.

As tabulated chemistry, virtual chemistry range of application depends on the flame ingredients retained to build up the reference database. When only premixed flamelet are used to train the virtual scheme, CO formation processes are not predicted in non-premixed flames. However, the addition of non-premixed flamelet archetype to the reference database improve the results. The main advantage of virtual schemes compared to tabulated chemistry is that the issues raised before are bypassed by the method. Indeed, virtual chemistry strategy does not require to transpose flame solutions from the physical space to a composition space whose coordinate identification is complex.

Appendix A. Optimization algorithm

This appendix gives details on the genetic optimization tool. A real encoded genetic algorithm is considered in this work as it is particularly suited for constrained, high-precision and multidimensional optimization problem [34]. Initialization, selection procedure, genetic operators and reduction technique used in the optimization code are discussed hereinafter.

The population initialization is performed using the classical Mersenne Twister pseudorandom numbers generator [69].

The selection operator is based on a stochastic binary tournament. This operator selects with a probability p_T the fittest individual of a couple of randomly chosen potential solutions. This simple and low CPU demanding algorithm enables an easy control of the selective pressure and population diversity by adjusting the value of the tournament probability p_T. In this work, the intermediate value $p_T = 0.7$ was found to adequately balance between strong selective pressure promoted with $p_T = 1.0$ (determinist selection) and weak selective pressure promoted with $p_T = 0.5$ (random selection).

The crossover operation considered in this study is the Simulated Binary Crossover (SBX) introduced by Deb and Agrawal [70]. Main advantage of this recombination operation is to avoid bias towards any parent solution. Moreover, as the children solutions has a spread which is proportional to that of the parent solutions,

solution dispersion reduces as generations evolve to ease convergence. Application of the SBX crossover is performed with a probability $\mathcal{P}_c$ equal to 0.7 to ensure a satisfactory exploitation of the evaluation step.

The non-uniform mutation operator proposed by Michalewicz [71] is used in this work. This dynamic mutation operator is designed to allow a fine local tuning of the population diversity with time. If the kth gene g_k of parent P is selected for mutation the gene k g_k' of the associated children C reads:

$$g_k' = \begin{cases} g_k + \Delta\left(n, g_k^{\max} - g_k\right) & \text{if } \mathcal{R} = 0 \\ g_k - \Delta\left(n, g_k - g_k^{\min}\right) & \text{if } \mathcal{R} = 1 \end{cases} \quad (A.1)$$

where n is the curent number of generations, the superscripts min and max denote the minimum and maximum bounds for the kth parameter to optimize, and $\mathcal{R}$ is a random number. The function $\Delta(n, y)$ returns a value in the range $[0, y]$ such that the probability of $\Delta(n, y)$ to be close to 0 increases when n increases. The function used by Martin [23] is considered. Each solution has a probability $\mathcal{P}_m = 0.1$ to mute. This value was found to allow a good balance between space exploitation and exploration.

A reduction operation operation relying on k-tournament selection is applied to select the individual retained for the next generation. To ensure population diversity the reduction operation prevents an individual to be selected twice in the new generation.

Appendix B. Product thermodynamic properties optimization

This appendix discusses the calibration procedure used to identify the virtual products thermodynamic properties. The in-house genetic algorithm described in Section 2.2 is used to identify the set of free parameters $\mathcal{X}$ that minimizes the cost function defined in Eq. (20) and expressed as:

$$\mathcal{E}_{\text{thermo}}^{\text{main}}(\mathcal{X})\left(N_p^{\nu_m}, \alpha_{P_k}^{\nu_m}(\phi_i), a_{IP_k}^{\nu_m}\right) = \sum_{i=1}^{N_c}\sum_{l=1}^{N_T}\left[\bar{a}_{IP}^{\nu_m}|^{eq}(\phi_i) - \sigma_l(\phi_i)\right] \quad (B.1)$$

where $\sigma_l(\phi_i) = \bar{a}_l^d|^{eq}(\phi_i) - \bar{a}_{IA}^{\nu_m}|^{eq}$. The function $\bar{a}_{IA}^{\nu_m}|^{eq}(\phi_i)$ is entirely defined by real species properties and equilibrium concentration of reactants, while $\bar{a}_l^d|^{eq}(\phi_i)$ is obtained through equilibrium calculations with detailed chemistry. Therefore, $\sigma_l(\phi_i)$ is known and constitutes the target coefficient of the optimization procedure. Figure B.20 shows the evolution of the 6 coefficients σ_l versus the equivalence ratio.

The term $\bar{a}_{IP}^{\nu_m}|^{eq}(\phi_i)$ is unknown and needs to be optimized in order to minimize the cost function $\mathcal{E}_{\text{thermo}}^{\text{main}}$ defined by Eq. (B.1):

$$\bar{a}_{IP}^{\nu_m}|^{eq}(\phi_i) = \sum_{k=1}^{N_p^{\nu_m}} a_{IP_k}^{\nu_m}\alpha_{P_k}^{\nu_m}Y_P^{\nu_m}|^{eq}(\phi_i) \quad \text{for} \quad l \in [1, N_T] \quad (B.2)$$

The optimization calculation requires the evaluation of $N_T \times N_p^{\nu_m}$ thermodynamic coefficients $a_{IP_k}^{\nu_m}$, and $(N_p^{\nu_m} - 1) * N_c$ stoichiometric coefficients $\alpha_{P_k}^{\nu_m}$. For only two products and $N_c = 31$ equivalence ratio conditions, 43 variables have therefore to be determined. To ease the optimization procedure, the problem is divided into two parts. We first consider that for each of $N_p^{\nu_m}$ products, a subset of N_θ thermodynamic coefficients $a_{IP_k}^{\nu_m}$ is known and ensure a perfect reproduction of the corresponding target coefficients over the whole flammability range. This hypothesis can be expressed through the following system presented in its general form for the equivalence ratio ϕ_i:

$$\begin{cases} \sum_{k=1}^{N_p^{\nu_m}} a_{1P_k}^{\nu_m}\alpha_{P_k}^{\nu_m}Y_P^{\nu_m}|^{eq}(\phi_i) = \sigma_1(\phi_i) \\ \dots \\ \sum_{k=1}^{N_p^{\nu_m}} a_{N_\theta P_k}^{\nu_m}\alpha_{P_k}^{\nu_m}Y_P^{\nu_m}|^{eq}(\phi_i) = \sigma_{N_\theta}(\phi_i) \end{cases} \quad (B.3)$$

With the arbitrary constraint $\sum_{k=1}^{N_p^{\nu_m}}\alpha_{P_k}^{\nu_m} = 1$, Eq. (B.3) can be rewritten:

$$\begin{cases} \sum_{k=1}^{N_p^{\nu_m}-1}\left[a_{1P_k}^{\nu_m}\alpha_{P_k}^{\nu_m}(\phi_i)\right] + a_{1P_{N_p}}^{\nu_m}\left(1 - \sum_{k=1}^{N_p^{\nu_m}-1}\alpha_{P_k}^{\nu_m}(\phi_i)\right) = \frac{\sigma_1}{Y_P^{\nu_m}|^{eq}}(\phi_i) \\ \dots \\ \sum_{k=1}^{N_p^{\nu_m}-1}\left[a_{N_\theta P_k}^{\nu_m}\alpha_{P_k}^{\nu_m}(\phi_i)\right] + a_{N_\theta P_{N_p}}^{\nu_m}\left(1 - \sum_{k=1}^{N_p^{\nu_m}-1}\alpha_{P_k}^{\nu_m}(\phi_i)\right) = \frac{\sigma_{N_\theta}}{Y_P^{\nu_m}|^{eq}}(\phi_i) \end{cases} \quad (B.4)$$

If $N_\theta = N_p^{\nu_m} - 1$, the system Eq. (B.4) exhibits $N_p^{\nu_m} - 1$ equations and $N_p^{\nu_m} - 1$ unknown functions $\alpha_{P_k}^{\nu_m}(\phi)$. The stoichiometric coefficients $\alpha_{P_k}^{\nu_m}(\phi_i)$ can be evaluated by inverting the N_c systems of Eq. (B.4). Thus for any set of $N_\theta = N_p^{\nu_m} - 1$ thermodynamic coefficients, the evolution of the product stoichiometric coefficients in the composition space can be calculated. However, the physical consistency (bounded behavior) of the resulting $\alpha_{P_k}^{\nu_m}(\phi)$ coefficients is not necessarily obtained. Then the identification of the best subset of $N_p^{\nu_m} - 1$ thermodynamic coefficients and associated $\alpha_{P_k}^{\nu_m}(\phi)$ is done through genetic optimization with the objective to respect the physical constraint: $0 < \alpha_{P_k}^{\nu_m}(\phi_i) < 1$. Practically, the physical behavior of the stoichiometric coefficients is ensured by minimizing the cost function $\mathcal{E}_{\text{thermo 1}}^{\text{main}}$:

$$\mathcal{E}_{\text{thermo 1}}^{\text{main}} = \sum_{k=1}^{N_p^{\nu_m}}\delta_{P_k} \quad \text{with} \quad \delta_{P_k} = \begin{cases} 0 & \text{if} \quad \alpha_{P_k}^{\nu_m}(\phi_i) \in]0; 1[\\ 1 & \text{else} \end{cases} \quad (B.5)$$

The second part of the optimization procedure aims at evaluating the $N_{\theta'} = N_T - N_\theta$ residual thermodynamic coefficients. The optimization algorithm is again used to minimize the fitness function $\mathcal{E}_{\text{thermo 2}}^{\text{main}}$:

$$\mathcal{E}_{\text{thermo 2}}^{\text{main}} = \sum_{i=1}^{N_c}\sum_{l=m}^{N_{\theta'}}\left[\bar{a}_{IP}^{\nu}|^{eq}(\phi_i) - \sigma_l(\phi_i)\right] \quad (B.6)$$

In practice, the choice of the N_θ thermodynamic coefficients optimized during the first stage of the procedure is important. Figure B.20 shows that three families of coefficients can be identified considering their evolution in the composition space. The coefficients σ_1, σ_3 and σ_5, belonging to the family called $\mathcal{F}_1$, feature a constant behavior for lean mixtures and the same increasing trend in the rich zone. The second family of coefficients $\mathcal{F}_2$, including the terms σ_2 and σ_4, is constant for lean injection conditions and shows a decrease with the equivalence ratio for rich mixtures. Finally the coefficient σ_6 presents a distinct behavior with a discontinuity near the stoichiometry. To summarize, if $N_\theta = 3$ thermodynamic coefficients are used to identify the evolution of $N_p^{\nu_m} = 4$ virtual product stoichiometric coefficients $\alpha_{P_k}^{\nu_m}(\phi_i)$, given the self-similar behavior of σ_l profiles, optimization of the $N_{\theta'} = 3$ remaining coefficients is therefore easier. If the N_θ chosen coefficients are for instance the first, second and last one, one can expect a rapid and efficient convergence of the optimization algorithm. As a conclusion, this a priori study shows a minimum number of four virtual products is required to describe the equilibrium state thermodynamic properties (c_p and h) of the mixture on the whole flammability range.
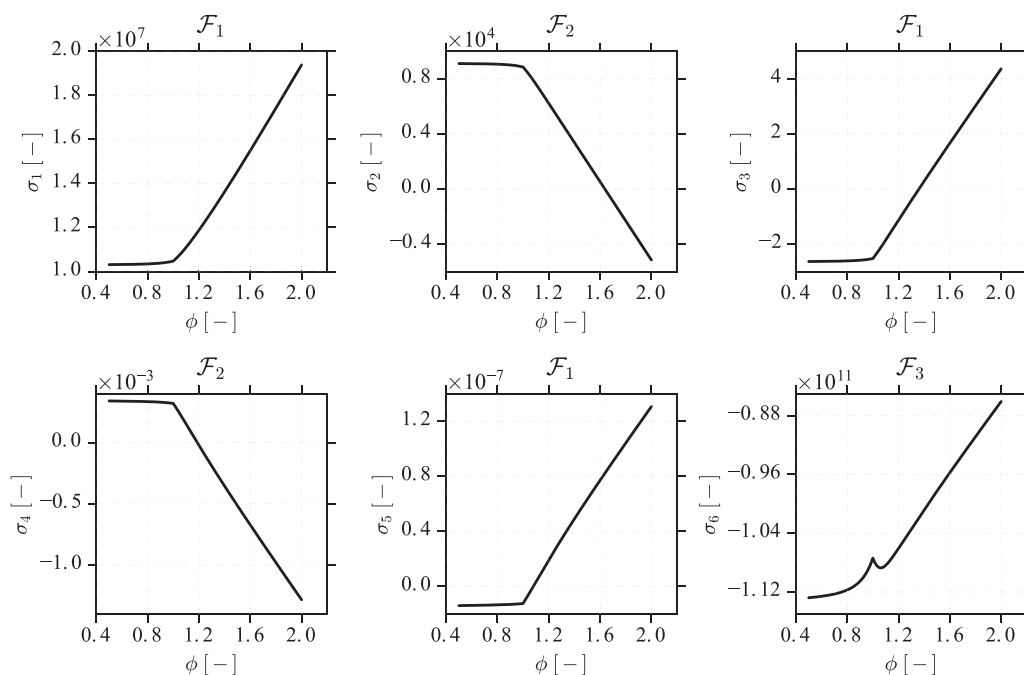
Fig. B.20. Evolution of the target coefficients σ_l versus the equivalence ratio.

Supplementary material

Supplementary material associated with this article can be found, in the online version, at doi:10.1016/j.cnsns.2019.01.021.

References

[1] A.H. Lefebvre, Gas turbine combustion, CRC Press, 1998.
[2] B. Fiorina, D. Veynante, S. Candel, Modeling combustion chemistry in large eddy simulation of turbulent flames, Flow Turbl. Combust. 94 (1) (2015) 3–42.
[3] N. Peters, Laminar diffusion flamelet models in non-premixed turbulent combustion, Prog. Energy Combust. Sci. 10 (3) (1984) 319–339.
[4] O. Gicquel, N. Darabiha, D. Thévenin, Laminar premixed hydrogen/air counterflow flame simulations using flame prolongation of ILDM with differential diffusion, Proc. Combust. Inst. 28 (2) (2000) 1901–1908.
[5] J.V. Oijen, F. Lammers, L. De Goey, Modeling of complex premixed burner systems by using flamelet-generated manifolds, Combust. Flame 127 (3) (2001) 2124–2134.
[6] C.D. Pierce, P. Moin, Progress-variable approach for large-eddy simulation of non-premixed turbulent combustion, J. Fluid Mech. 504 (2004) 73–97.
[7] B. Fiorina, O. Gicquel, L. Vervisch, S. Carpentier, N. Darabiha, Approximating the chemical structure of partially premixed and diffusion counterflow flames using FPI flamelet tabulation, Combust. Flame 140 (3) (2005) 147–160.
[8] B. Franzelli, B. Fiorina, N. Darabiha, A tabulated chemistry method for spray combustion, Proc. Combust. Inst. 34 (1) (2013) 1659–1666.
[9] S. Vajda, P. Valko, T. Turányi, Principal component analysis of kinetic models, Int. J. Chem. Kinet. 17 (1) (1985) 55–81.
[10] T. Lu, C.K. Law, A directed relation graph method for mechanism reduction, Proc. Combust. Inst. 30 (1) (2005) 1333–1341.
[11] P. Pepiot-Desjardins, H. Pitsch, An efficient error-propagation-based reduction method for large chemical kinetic mechanisms, Combust. Flame 154 (2008) 67–81.
[12] S. Lam, Using CSP to understand complex chemical kinetics, Combust. Sci. Technol. 89 (5–6) (1993) 375–404.
[13] V. Lepage, Elaboration d'une méthode de réduction de schémas cinétiques détaillés. Application aux mécanismes de combustion du gaz naturel et du n-décane, Université d'Orléans, 2000 Ph.D. thesis.
[14] T. Løvås, D. Nilsson, F. Mauss, Automatic reduction procedure for chemical mechanisms applied to premixed methane/air flames, Proc. Combust. Inst. 28 (2) (2000) 1809–1815.
[15] J. Luche, Elaboration of reduced kinetic models of combustion. Application to a kerosene mechanism, Université d'Orléans, 2003 Ph.D. thesis.
[16] T. Lu, C.K. Law, A criterion based on computational singular perturbation for the identification of quasi steady state species: a reduced mechanism for methane oxidation with NO chemistry, Combust. Flame 154 (4) (2008) 761–774.
[17] T. Jaravel, E. Riber, B. Cuenot, G. Bulat, Large eddy simulation of an industrial gas turbine combustor using reduced chemistry with accurate pollutant prediction, Proc. Combust. Inst. 36 (3) (2017) 3817–3825.
[18] N. Jaouen, L. Vervisch, P. Domingo, G. Ribert, Automatic reduction and optimisation of chemistry for turbulent combustion modelling: impact of the canonical problem, Combust. Flame 175 (2017) 60–79.
[19] C.K. Westbrook, F.L. Dryer, Simplified reaction mechanisms for the oxidation of hydrocarbon fuels in flames, Combust. Sci. Technol. 27 (1–2) (1981) 31–43.
[20] W. Jones, R. Lindstedt, Global reaction schemes for hydrocarbon combustion, Combust. Flame 73 (3) (1988) 233–249.
[21] B. Franzelli, E. Riber, M. Sanjosé, T. Poinsot, A two-step chemical scheme for kerosene–air premixed flames, Combust. Flame 157 (7) (2010) 1364–1373.
[22] W. Polifke, W. Geng, K. Döbeling, Optimization of rate coefficients for simplified reaction mechanisms with genetic algorithms, Combust. Flame 113 (1–2) (1998) 119–134.
[23] C.-E. Martin, Etude énergétique des instabilités thermo-acoustiques et optimisation génétique des cinétiques réduites, Institut National Polytechnique de Toulouse, 2005 Ph.D. thesis.
[24] A. Abou-Taouk, S. Sadasivuni, D. Lörstad, L.-E. Eriksson, Evaluation of global mechanisms for LES analysis of SGT-100 DLE combustion system. Proceedings of the ASME Turbo Expo 2013: Turbine Technical Conference and Exposition. Volume 1B: Combustion, Fuels and Emissions. San Antonio, Texas, USA. June 3–7, 2013. V01BT04A036. ASME. https://doi.org/10.1115/GT2013-95454.
[25] B. Farcy, A. Abou-Taouk, L. Vervisch, P. Domingo, N. Perret, Two approaches of chemistry downsizing for simulating selective non catalytic reduction deno x process, Fuel 118 (2014) 291–299.
[26] S. Hermeth, G. Staffelbach, L.Y. Gicquel, V. Anisimov, C. Cirigliano, T. Poinsot, Bistable swirled flames and influence on flame transfer functions, Combust. Flame 161 (1) (2014) 184–196.
[27] A. Abou-Taouk, B. Farcy, P. Domingo, L. Vervisch, S. Sadasivuni, L.E. Eriksson, Optimized reduced chemistry and molecular transport for Large Eddy Simulation of partially premixed combustion in a gas turbine, Combust. Sci. Technol. 188 (1) (2016) 21–39.
[28] P.S. Volpiani, T. Schmitt, D. Veynante, Large eddy simulation of a turbulent swirling premixed flame coupling the TFLES model with a dynamic wrinkling formulation, Combust. Flame 180 (2017) 124–135.
[29] M. Cailler, N. Darabiha, D. Veynante, B. Fiorina, Building-up virtual optimized mechanism for flame modeling, Proc. Combust. Inst. 36 (1) (2017) 1251–1258.
[30] A. Er-raiy, Z. Bouali, J. Réveillon, A. Mura, Optimized single-step (oss) chemistry models for the simulation of turbulent premixed flame propagation, Combust. Flame 192 (2018) 130–148.
[31] M. Cavazzuti, Deterministic optimization, Springer, 2013, pp. 77–102.
[32] G.S. Beveridge, R.S. Schechter, Optimization, theory and practice, McGraw-Hill (1970).
[33] J.E. Gentle, W.K. Härdle, Y. Mori, Handbook of computational statistics: concepts and methods, Springer Science & Business Media, 2012.
[34] L. Elliott, D. Ingham, A. Kyne, N. Mera, M. Pourkashanian, C. Wilson, Genetic algorithms for optimisation of chemical kinetics reaction mechanisms, Prog. Energy Combust. Sci. 30 (3) (2004) 297–328.
[35] S. Harris, L. Elliott, D. Ingham, M. Pourkashanian, C. Wilson, The optimisation of reaction rate parameters for chemical kinetic modelling of combustion using genetic algorithms, Comput. Methods Appl. Mech. Eng. 190 (8) (2000) 1065–1090.

[36] N. Jaouen, L. Vervisch, P. Domingo, Auto-thermal reforming (ATR) of natural gas: an automated derivation of optimised reduced chemical schemes, Proc. Combust. Inst. 36 (3) (2017) 3321–3330.

[37] Z. Michalewicz, M. Schoenauer, Evolutionary algorithms for constrained parameter optimization problems, Evolutionary Comput. 4 (1) (1996) 1–32.

[38] C. Darwin, The origin of species by means of natural selection: or, the preservation of favored races in the struggle for life, 1859,

[39] J.H. Holland, Adaptation in natural and artificial systems: an introductory analysis with applications to biology, control artificial intelligence, 1975.

[40] D.E. Goldberg, Genetic algorithms in search, optimization and machine learning, 1st ed., Boston, MA, USA, 1989.

[41] N. Darabiha, S. Candel, The influence of the temperature on extinction and ignition limits of strained hydrogen-air diffusion flames, Combust. Sci. Technol. 86 (1–6) (1992) 67–85.

[42] T. Poinsot, D. Veynante, Theoretical and numerical combustion. Third ed. by T. Poinsot, 2012,

[43] R.S. Barlow, M.J. Dunn, M.S. Sweeney, S. Hochgreb, Effects of preferential transport in turbulent bluff-body-stabilized lean premixed CH_4/air flames, Combust. Flame 159 (8) (2012) 2563–2575.

[44] M.S. Sweeney, S. Hochgreb, M.J. Dunn, R.S. Barlow, The structure of turbulent stratified and premixed methane/air flames I: non-swirling flows, Combust. Flame 159 (9) (2012) 2896–2911.

[45] A. Liñán, F.A. Williams, Fundamental aspects of combustion, Oxford University Press, New York, NY, United States, 1993.

[46] G.P. Smith, D.M. Golden, M. Frenklach, B. Eiteener, M. Goldenberg, C.T. Bowman, R.K. Hanson, W.C. Gardiner, V.V. Lissianski, Z.W. Qin, Gri-mech 3.0, 2011, http://www.me.berkeley.edu/gri_mech.

[47] J.O. Hirschfelder, C.F. Curtiss, R.B. Bird, M.G. Mayer, Molecular theory of gases and liquids 26 (1954).

[48] P. Pepiot, Automatic strategies to model transportation fuel surrogates, Stanford University, 2008 Ph.D. thesis.

[49] R. Kee, H. Dwyer, Review of stiffness and implicit finite difference methods in combustion modeling, Sandia National Labs., Livermore, CA, USA (1980). Technical Report

[50] U. Pruefert, F. Hunger, C. Hasse, The analysis of chemical time scales in a partial oxidation flame, Combust. Flame 161 (2) (2014) 416–426.

[51] S. Lam, Singular perturbation for stiff equations using numerical methods, Recent Advances in the Aerospace Sciences, Springer (1985), pp. 3–19.

[52] U. Maas, S.B. Pope, Simplifying chemical kinetics: intrinsic low-dimensional manifolds in composition space, Combust. Flame 88 (3) (1992) 239–264.

[53] T. Løvås, F. Mauss, C. Hasse, N. Peters, Development of adaptive kinetics for application in combustion systems, Proc. Combust. Inst. 29 (1) (2002) 1403–1410.

[54] J. Caudal, B. Fiorina, M. Massot, B. Labégorre, N. Darabiha, O. Gicquel, Characteristic chemical time scales identification in reactive flows, Proc. Combust. Inst. 34 (1) (2013) 1357–1364.

[55] B. Franzelli, E. Riber, L.Y. Gicquel, T. Poinsot, Large eddy simulation of combustion instabilities in a lean partially premixed swirled flame, Combust. Flame 159 (2) (2012) 621–637.

[56] L.M. Somers, L. De Goey, A numerical study of a premixed flame on a slit burner, Combust. Sci. Technol. 108 (1–3) (1995) 121–132.

[57] B. Fiorina, R. Baron, O. Gicquel, D. Thevenin, S. Carpentier, N. Darabiha, Modelling non-adiabatic partially premixed flames using flame-prolongation of ILDM, Combust. Theory Model. 7 (3) (2003) 449–470.

[58] V. Moureau, P. Domingo, L. Vervisch, Design of a massively parallel CFD code for complex geometries, C. R. Acad. Sci. 339 (2–3) (2011) 141–148.

[59] M. Kraushaar, Application of the compressible and low-Mach number approaches to large eddy simulation of turbulent flows in aero-engines, Institut National Polytechnique de Toulouse, 2011 Ph.D. thesis.

[60] C. Saggese, S. Ferrario, J. Camacho, A. Cuoci, A. Frassoldati, E. Ranzi, H. Wang, T. Faravelli, Kinetic modeling of particle size distribution of soot in a premixed burner-stabilized stagnation ethylene flame, Combust. Flame 162 (9) (2015) 3356–3369.

[61] H. Wang, X. You, A.V. Joshi, S.G. Davis, A. Laskin, F. Egolfopoulos, C.K. Law, USC mech version II. High-temperature combustion reaction model of H2/CO/C1-C4 compounds, 2007, http://ignis.usc.edu/USC_Mech_II.htm.

[62] A. Stagni, A. Cuoci, A. Frassoldati, T. Faravelli, E. Ranzi, Lumping and reduction of detailed kinetic schemes: an effective coupling, Ind. Eng. Chem. Res. 53 (22) (2013) 9004–9016.

[63] P. Dagaut, On the kinetics of hydrocarbons oxidation from natural gas to kerosene and diesel fuel, Phys. Chem. Chem. Phys. 4 (11) (2002) 2079–2094.

[64] V. Bykov, U. Maas, The extension of the ILDM concept to reaction–diffusion manifolds, Combust. Theory Model. 11 (6) (2007) 839–862.

[65] P.-D. Nguyen, L. Vervisch, V. Subramanian, P. Domingo, Multidimensional flamelet-generated manifolds for partially premixed combustion, Combust. Flame 157 (1) (2010) 43–61.

[66] M. Ihme, L. Shunn, J. Zhang, Regularization of reaction progress variable for application to flamelet-based combustion models, J. Comput. Phys. 231 (23) (2012) 7715–7721.

[67] S. Niu, Y.-,L. Vervisch, P.D. Tao, An optimization-based approach to detailed chemistry tabulation: automated progress variable definition, Combust. Flame 160 (4) (2013) 776–785.

[68] A. Scholtissek, P. Domingo, L. Vervisch, C. Hasse, A self-contained progress variable space solution method for thermochemical variables and flame speed in freely-propagating premixed flamelets, Proc. Combust. Inst. 37 (2) (2018) 1529–1536.

[69] M. Matsumoto, T. Nishimura, Mersenne twister: a 623-dimensionally equidistributed uniform pseudo-random number generator, ACM Trans. Model. Comput. Simul. 8 (1) (1998) 3–30.

[70] K. Deb, R.B. Agrawal, Simulated binary crossover for continuous search space, Complex Syst. 9 (2) (1995) 115–148.

[71] Z. Michalewicz, Genetic algorithms+ data structures = evolution programs, Springer, 2013.